CHEMISTRY OF MATERIALS

Perspective

pubs.acs.org/cm

Between the Sheets: Postsynthetic Transformations in Hybrid Perovskites

Ian C. Smith,[†] Matthew D. Smith,[†] Adam Jaffe,[†] Yu Lin,[†,‡] and Hemamala I. Karunadasa*[,†]

[†]Department of Chemistry, Stanford University, Stanford, California 94305, United States

[‡]Stanford Institute for Materials and Energy Sciences, SLAC National Accelerator Laboratory, Menlo Park, California 94025, United States

ABSTRACT: Hybrid perovskites combine the optical and electronic versatility of ionic inorganic solids with the synthetic diversity and tunability of covalent organic molecules. Their multicomponent, crystalline architectures, incorporating a wide array of metals, ligands, and organic molecules, can be synthetically fine-tuned to accommodate diverse target technologies. In this Perspective, we highlight how the utility of hybrid perovskites can be further extended through chemical and physical postsynthetic transformations, with an emphasis on the design of functional solids. We describe strategies that we and other researchers have developed for using the parent perovskite to direct the structure or morphology of the product. We further show how the perovskite structure provides a unique reaction vessel for performing chemical transformations that cannot be accessed through conventional methods. We hope this Perspective motivates both organic and inorganic chemists to further expand the versatility of these technologically important hybrids, whose physical and electronic properties are highly amenable to synthetic design.

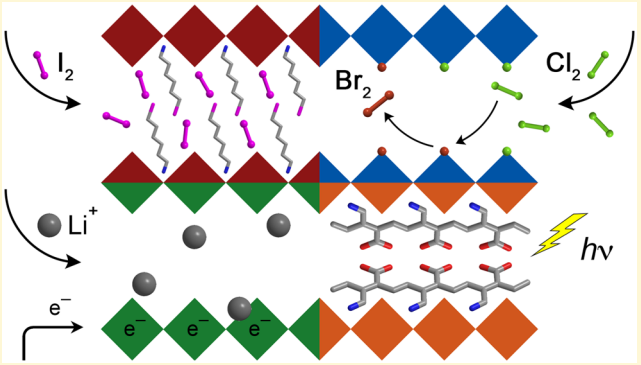

1. INTRODUCTION

Postsynthetic transformations of solids allow for the parent structure to fully or partially template the product, affording new structures and morphologies not accessible through traditional means. For example, postsynthetic ion-exchange reactions in zeolitic frameworks,[1] postsynthetic metalation,[2] transmetalation,[3,4] anion-exchange,[5] and polymerization[6] reactions in metal−organic frameworks,[7] and postsynthetic metal-ion-exchange in metal-chalcogenide nanoparticles[8] have substantially expanded the structural and functional diversity of these materials. Similarly, the organic and inorganic components of hybrid perovskites provide an ideal platform for developing postsynthetic strategies that expand their phase space. In contrast to primarily covalent framework materials, the distinctly ionic and covalent bonding found in these materials provide additional flexibility for synthetic tuning of their electronic structures. Hybrid perovskites therefore offer a unique and underutilized space to exploit postsynthetic transformations that target new physical, electronic, and optical properties for both applied and fundamental studies.

This Perspective provides an overview of research on the postsynthetic chemistry of these versatile solids and outlines our explorations in the field, with an emphasis on achieving targeted properties for functional materials such as solar-cell absorbers, phosphors, battery electrodes, and sorbents for atmospheric pollutants. Although the facile solution-state self-assembly of hybrid perovskites under ambient conditions is an advantage with respect to inexpensive and scalable manufacture, it also limits the number of accessible structures and compositions. Because these materials typically crystallize from their precursor salt solutions, the favored structure is often dictated by the kinetics of crystallization, although changing reaction parameters such as temperature, pressure, and pH can provide some thermodynamic control. To further exploit the structural versatility of hybrid perovskites, herein we describe postsynthetic small-molecule intercalation, small-molecule chemisorption, polymerization, ion exchange, electrochemical ion insertion, and material compression.

1.1. Structure.

This work focuses on halide perovskites, which are structurally analogous to the more common oxide perovskites.[9] Three-dimensional (3D) halide perovskites adopt the $CaTiO_3$ structure, where the inorganic sublattice consists of corner-sharing metal-halide octahedra. The inorganic sublattice of two-dimensional (2D) halide perovskites can be derived from this 3D structure by conceptually slicing along different crystallographic planes. Importantly, unlike the high-temperature (>500 °C) routes often required for oxide perovskites, halide perovskites typically form under ambient conditions in organic or aqueous solution. These milder conditions allow for the incorporation of organic molecules into halide perovskites,

Received: December 20, 2016
Revised: February 15, 2017
Published: February 16, 2017

DOI: 10.1021/acs.chemmater.6b05395
Chem. Mater. 2017, 29, 1868−1884

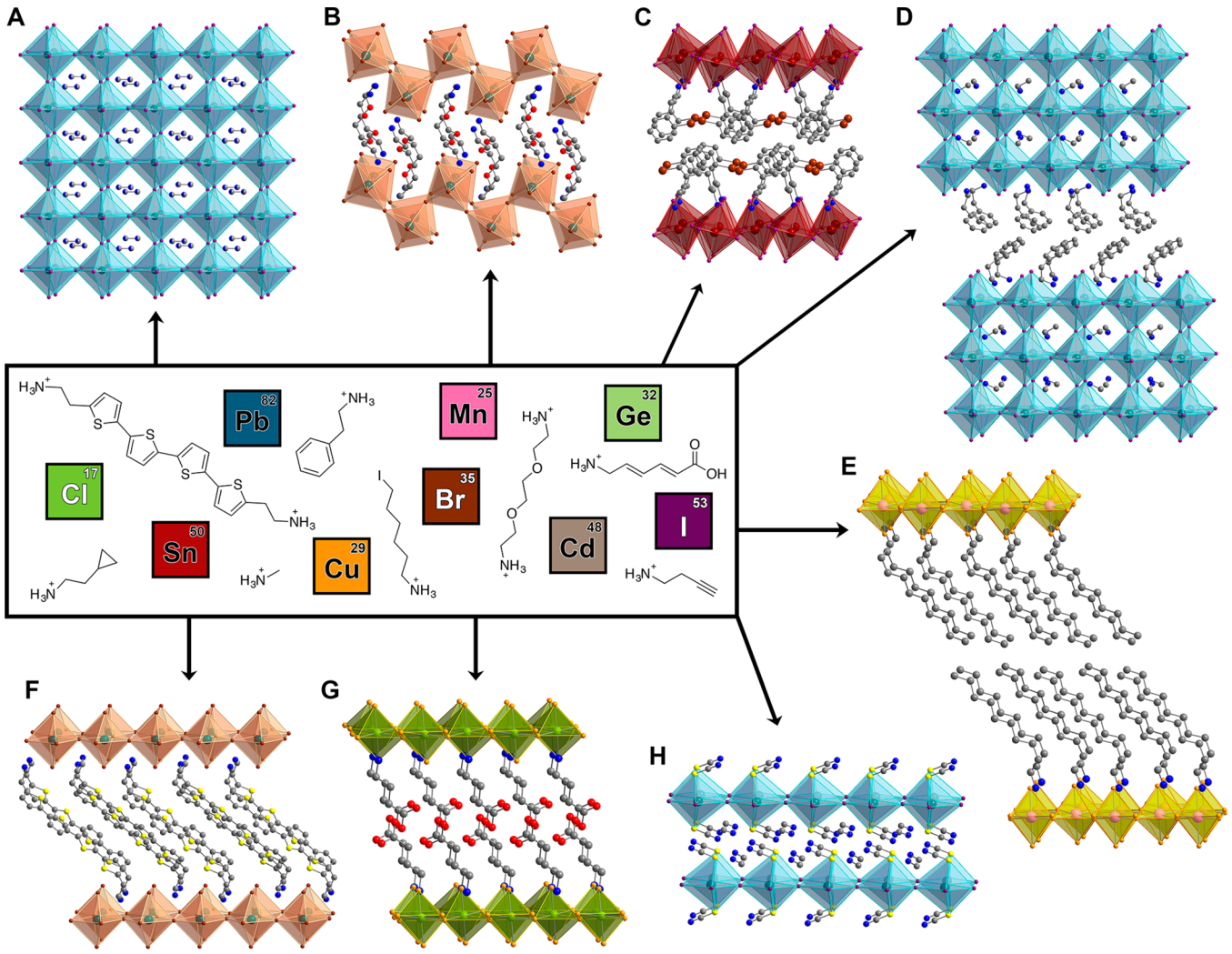

Figure 1. Crystal structures representing a subset of architectures and compositions that can be achieved with hybrid perovskites. (A) 3D $(MA)[PbI_3]$;[120] (B) n = 1 $(EDBE)[PbBr_4]$ with (110) inorganic sheets and an organic monolayer;[10] (C) n = 1 $(o\text{-BrPEA})_2[SnI_4]$ with (001) inorganic sheets and an organic bilayer;[11] (D) n = 3 $(PEA)_2(MA)_2[Pb_3I_{10}]$;[12] (E) n = 1 $(C10)_2[MnCl_4]$;[13] (F) n = 1 $(AEQT)[PbBr_4]$;[14] (G) n = 1 $(GABA)_2[CuCl_4]$;[15] (H) pseudohalide-containing n = 1 $(MA)_2[PbI_2(SCN)_2]$.[16] Dark green, dark red, light green, pink, purple, brown, orange, yellow, red, blue, and gray spheres represent Pb, Sn, Cu, Mn, I, Br, Cl, S, O, N, and C atoms, respectively. Disordered atoms and hydrogens omitted for clarity. MA = methylammonium; EDBE = 2,2′-(ethylenedioxy)bis(ethylammonium); *o*-BrPEA = 2-bromophenethylammonium; PEA = phenethylammonium; C10 = decylammonium; AEQT = 5,5‴-bis(ethylammonium)-2,2′:5′,2″:5″,2‴-quaterthiophene; GABA = γ-ammoniobutyric acid.

affording single-phase organic–inorganic hybrids. Smaller organic cations reside in the cavities of 3D hybrid perovskites (Figure 1A), whereas larger organic cations partition the inorganic sheets in 2D perovskites.[10−16] Layered perovskites can feature an organic monolayer (Figure 1B,F) with the formula $R[BX_4]$ (R = divalent organic cation, B = metal cation, X = halide) or an organic bilayer (Figure 1C,D,E,G,H) with the formula $R'_2[BX_4]$ (R′ = monovalent organic cation). Unlike in the 3D structure, which can only accommodate small organic or inorganic cations, the 2D perovskite exhibits a far greater tolerance for a wide range of organic functionalities. This has allowed for the synthesis of perovskites containing alkenyl,[17] alkynyl,[17] aryl,[18] carboxyl,[19] cycloalkyl,[20] halo,[17,21] heterocycle,[22] hydroxyl,[21] nitrilo,[23] and silyl[24] groups. These materials provide the basis for expanding the diversity of hybrid perovskites by developing reactions that leverage the inherent reactivity of these functional groups. The inorganic framework of 2D perovskites can be further tuned by using a mixture of small and large organic cations. Here, the small cations template thick 2D slabs of the inorganic layers, whereas the larger cations partition the inorganic lattice. The thickness of the inorganic sheets can therefore be controlled by the ratio of small to large cations (Figure 1D). These 2D perovskites have the general formula $R_2A_{n-1}[M_nX_{3n+1}]$ (R = organic cation that partitions the inorganic sheets, A = cation that is incorporated into the inorganic sheets, M = metal, X = halide) where n denotes the number of metal-halide sheets in each inorganic layer.[25,26]

1.2. Optical and Electronic Properties. Recent work on halide perovskites has primarily focused on the 3D perovskite $R[PbI_3]$ (R = monovalent cation), which has shown exceptional performance for photovoltaic[27−31] and other optoelectronic applications.[32−35] Their 2D analogs exhibit contrasting photophysical properties that have been studied for decades[36,37] and developed for applications in organic–inorganic electronics.[38]

DOI: 10.1021/acs.chemmater.6b05395
Chem. Mater. 2017, 29, 1868−1884

The 3D lead-halide perovskites exhibit direct bandgaps, small exciton binding energies (E_b, i.e., attraction between photogenerated electrons and holes), and long carrier recombination lifetimes, which are ideal for photovoltaic applications.[39] In contrast, the 2D lead-halide perovskites are wide-bandgap excitonic semiconductors with high E_b values (of ca. 300 meV for Pb−I perovskites).[37,40] The high oscillator strength of excitons in 2D lead-halide perovskites affords strong, room-temperature photoluminescence (PL). This has led to their study as candidates for green phosphor[41] and light-emitting[42] diode applications. Our lab has examined the phenomenon of exciton self-trapping[43] in layered Pb−Br and Pb−Cl perovskites that emit white light, where we hypothesized that the broadband emission stems from excitons that are stabilized by excited-state lattice distortions.[10,44,45]

Substantial electronic diversity exists even within 2D perovskites. For example, the 2D Cu−Cl perovskites are Mott/charge-transfer insulators.[46−48] Even within 2D lead-halide perovskites, the optical bandgap (E_g) and E_b can be systematically tuned by changing the thickness of the inorganic layer in $R_2A_{n-1}[M_nX_{3n+1}]$. Importantly, as n increases and the inorganic sheets in 2D perovskites become thicker, they approach the properties of the 3D perovskite, while the organic layers provide additional functionality. For example, we demonstrated that the inorganic layers in n = 3 Pb−I perovskites (Figure 1D) could absorb sunlight to generate photocurrent, while hydrophobic molecules in the organic layers ($(C_6H_5(CH_2)_2NH_3^+$,[12] 4-$FC_6H_4(CH_2)_2NH_3^+$[49]) substantially improved moisture resistance compared to the 3D perovskite absorber $(MA)[PbI_3]$ ($MA = CH_3NH_3^+$).

2. SMALL-MOLECULE INTERCALATION

Layered hybrid perovskites are typically nonporous solids.[17] A recently reported exception contains oligomeric propylammonium silsesquioxane cations in the organic layer, affording BET surface areas of up to 205 $m^2 \cdot g^{-1}$.[24] Despite this lack of porosity, weakly interacting organic bilayers allow for the entry of small molecules as the structure expands along the direction perpendicular to the sheets (Figure 2). Indeed, early studies

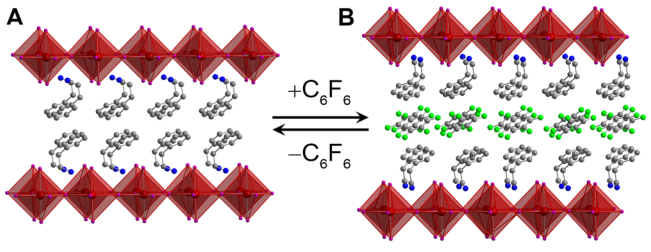

Figure 2. X-ray crystal structures of (A) $(C_6H_5(CH_2)_2NH_3)_2[SnI_4]$[53] and (B) its C_6F_6-intercalated product $(C_6H_5(CH_2)_2NH_3)_2[SnI_4]\cdot(C_6F_6)$.[18] Red, purple, lime, blue, and gray spheres represent Sn, I, F, N, and C, respectively. Disordered atoms and hydrogens omitted for clarity.

have attributed a paraffinic quality to long alkyl chains in the organic layers of 2D hybrid perovskites (Figure 1E), suggesting the potential for "solubilizing" small molecules.[50,51] Work by our group[52] and others[18,51] has used this trait to intercalate a range of molecules within the organic layers of 2D perovskites. Weak electrostatic[51] or stronger fluoroaryl−aryl[18] interactions have been used to stabilize small aliphatic or aromatic intercalants, where the guest molecules primarily induce structural changes. Our recent results extend this work and demonstrate that intercalants in the organic layers can significantly alter the photophysical properties of the inorganic layers.[52]

2.1. Intercalation: Structural Effects. The densely packed organic cations in 2D perovskites dictate that the unit cell must expand in the direction perpendicular to the inorganic sheets to accommodate the guests. This type of intercalation requires perovskites with an organic bilayer. This effect was first shown by Dolzhenko and co-workers in $(C_{10}H_{21}NH_3)_2[CdCl_4]$, where the interlayer spacing increased by 3.65 or 3.75 Å upon exposure of the perovskite to 1,2-dichlorobenzene or 1-chloronaphthalene, respectively.[51] Mitzi and co-workers subsequently determined the crystal structures of two Sn−I perovskites intercalated with hexafluorobenzene and benzene to afford the perovskites $(C_6H_5(CH_2)_2NH_3)_2[SnI_4]\cdot(C_6F_6)$ (Figure 2B) and $(C_6F_5(CH_2)_2NH_3)_2[SnI_4]\cdot(C_6H_6)$, respectively.[18] The single-crystal structures of these guest-containing perovskites enabled a more detailed analysis of the structural effects of intercalation. In addition to an expansion of the interlayer spacing by 4.3 Å in $(C_6H_5(CH_2)_2NH_3)_2[SnI_4]\cdot(C_6F_6)$ and 3.25 Å in $(C_6F_5(CH_2)_2NH_3)_2[SnI_4]\cdot(C_6H_6)$, the inorganic layers also distort in response to intercalation. In $(C_6H_5(CH_2)_2NH_3)_2[SnI_4]$,[53] the average Sn−I bond length increases slightly from 3.144 to 3.152 Å upon C_6F_6 intercalation, while the Sn−(μ-I)−Sn bond angle shows a substantial deviation from linearity. The optical response to these structural changes is described in Section 2.2.

Motivated by these studies, we decided to expand the scope of intercalants to more polarizable small molecules. The electronic and optical consequences of increasing the polarizability of the organic layers are discussed in Section 2.2. Under an I_2 atmosphere, thin films of $(C_6H_{13}NH_3)_2[PbI_4]$[54] (hereafter $(C_6)_2[PbI_4]$) change color from orange to red. Powder X-ray diffraction (PXRD) measurements on oriented thin films revealed an increase in the interlayer spacing of ca. 4 Å. However, these films rapidly reverted to the parent perovskite when removed from an I_2 atmosphere. To further stabilize the intercalated I_2, we then examined the perovskite $(IC_6H_{12}NH_3)_2[PbI_4]$[21] (hereafter $(IC_6)_2[PbI_4]$). Here, we hoped to use the terminal iodoalkyl groups in the organic layers (Figure 3A) to potentially stabilize the intercalated I_2 through attractive noncovalent interactions.

Intercalation of I_2 into $(IC_6)_2[PbI_4]$ resulted in a 5.5 Å (33%) increase in the interlayer spacing. We determined the structure of this metastable compound using density functional theory, starting from a hypothetical guess structure with two iodine atoms added per iodoalkyl group. Geometry optimization revealed the structure of the new perovskite $(IC_6H_{12}NH_3)_2[PbI_4]\cdot 2I_2$ (hereafter $(IC_6)_2[PbI_4]\cdot 2I_2$) containing I_2 molecules that interact with both the apical iodides of the inorganic layer as well as the terminal iodoalkyl groups in the organic layer (Figure 3B). The interlayer spacing derived from the calculated structure agrees well with the experimental value obtained from PXRD. Interestingly, here we postsynthetically access a perovskite that is structurally related to perovskites containing more complex terminal anions in the inorganic layers, such as the triiodides and thiocyanates in $(H_3N(CH_2)_8NH_3)_2[(Au^{I}I_2)(Au^{III}I_4)(I_3)_2]$[55] and $(CH_3NH_3)_2[PbI_2(SCN)_2]$,[16] respectively.

A common feature of intercalation in perovskites appears to be their reversibility (on the time scale of minutes to hours) upon removal from an environment of the guest. However,

DOI: 10.1021/acs.chemmater.6b05395
Chem. Mater. 2017, 29, 1868−1884

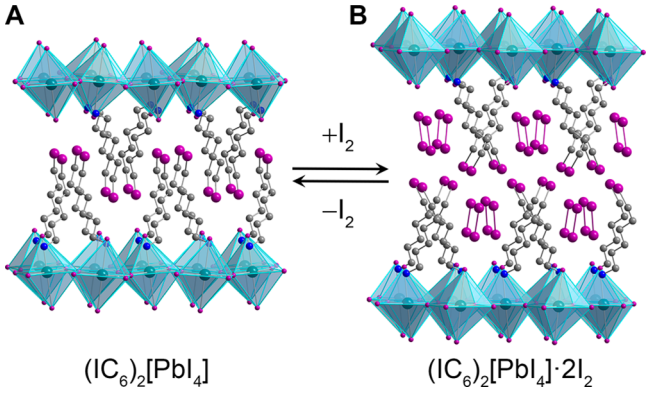

Figure 3. (A) Room-temperature X-ray crystal structure of $(IC_6)_2[PbI_4]$. (B) Geometry-optimized structure of the I_2-intercalated phase $(IC_6)_2[PbI_4]\cdot 2I_2$. Dark green, purple, blue, and gray spheres represent Pb, I, N, and C atoms, respectively. Disordered atoms and hydrogens omitted for clarity. Adapted from ref 52 with permission. Copyright 2016 Royal Society of Chemistry.

stronger interactions between the host and guests can be designed to stabilize the intercalated material. For example, I_2 retention time increases 4-fold in the perovskite $(IC_6)_2[PbI_4]\cdot 2I_2$ compared to $(C_6)_2[PbI_4]\cdot xI_2$, likely owing to the presence of I···I interactions between inorganic terminal iodides, organoiodines, and the I_2 guest molecules. Solid-state packing interactions between the intercalants can also extend the lifetime of the intercalated product as well as stabilize molecules that are unstable in solution. For example, vicinal diiodoalkane groups, which are unstable in solution, are stabilized in the organic layers of perovskites (described in Section 3.1.3).[17] This is likely due to packing interactions between the organoiodines within the perovskite.

The stabilizing environments discussed here can be extended for new perovskite intercalation compounds. Other bonding types, such as hydrogen bonding, Lewis donor−acceptor interactions, $\pi-\pi$ interactions between extended aromatic systems, and electrostatic interactions between polarizable groups (e.g., S−S interactions) are important targets to explore for these postsynthetic strategies.

2.2. Intercalation: Electronic Effects. Intercalant molecules can influence the electronic structure of layered perovskites primarily through two means: (1) distorting the inorganic framework and (2) interacting electronically with the inorganic layers. The first case is exemplified by the intercalation of hexafluorobenzene in $(C_6H_5(CH_2)_2NH_3)_2[SnI_4]$. Optical absorption spectroscopy of thin films reveals that the energy of the excitonic absorbance peak in $(C_6H_5(CH_2)_2NH_3)_2[SnI_4]\cdot(C_6F_6)$ is blueshifted by 45 meV compared to $(C_6H_5(CH_2)_2NH_3)_2[SnI_4]$. This blueshift has been correlated with increased deviation of the Sn−(μ-I)−Sn bond angles from linearity.[56] The second case occurs when intercalant molecules do not significantly distort the inorganic layers, yet directly affect their electronic properties. Because of the alternating stacks of organic and inorganic layers, perovskites can be considered as quantum-well-like structures, where the excitons reside in the inorganic "well" layers and the organic cations comprise the "barrier" layers.[37,57] These alternating layers affect two cooperative phenomena that promote the exceptionally large E_b in 2D perovskites: quantum confinement and dielectric confinement.[37,58] The inorganic layers confine the exciton's wave function to two dimensions,[59] increasing E_b by a factor of 4 relative to a 3D perovskite through quantum confinement.[60] Dielectric confinement[61,62] arises from the mismatch between high-frequency dielectric constants (ε_∞) of the inorganic and organic layers, and is greatly influenced by the composition of the organic layer. The less polarizable (low ε_∞) organic layer[37] poorly screens the Coulombic attraction between photogenerated electrons and holes in the inorganic layer, further increasing E_b. We therefore sought to determine if modifying the dielectric response of these materials by intercalating polarizable small molecules into the organic layers could substantially change the perovskites' electronic confinement.[52]

Upon exposure to I_2, the excitonic absorption band of the perovskite $(IC_6)_2[PbI_4]$ redshifts, accompanied by the growth of new above-gap absorption bands at 3−5 eV (Figure 4A) that

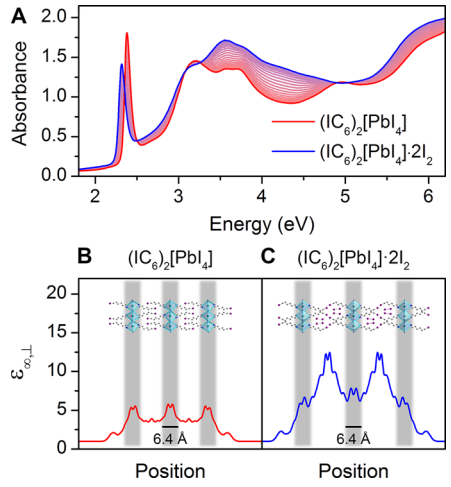

Figure 4. (A) In situ optical absorbance spectra of $(IC_6)_2[PbI_4]$ as it absorbs I_2 and forms $(IC_6)_2[PbI_4]\cdot 2I_2$. Calculated high-frequency dielectric constant perpendicular to the inorganic sheets ($\varepsilon_{\perp,\infty}$) in (B) $(IC_6)_2[PbI_4]$ and (C) $(IC_6)_2[PbI_4]\cdot 2I_2$. Adapted from ref 52 with permission. Copyright 2016 Royal Society of Chemistry.

we assigned to I_2-based transitions, based on calculated absorbance spectra.[52] Low-temperature optical absorbance spectra revealed that E_g decreases from 2.56 to 2.49 eV with I_2 intercalation. Typical n = 1 Pb−I perovskites have E_b values of ca. 300 meV.[37,40] The atypically low E_b of the perovskite $(PEA)_2[PbI_4]$ (PEA = $C_6H_5(CH_2)_2NH_3^+$) of 220 meV has been attributed to the greater polarizability of the aromatic groups in the organic layers, compared to alkyl groups.[63] The perovskite $(IC_6)_2[PbI_4]$ has a similarly low E_b of 230 meV, likely due to the polarizability of the iodoalkyl groups in the organic layers. Intercalation of I_2 further decreases E_b in $(IC_6)_2[PbI_4]\cdot 2I_2$ to 180 meV, the lowest E_b for an n = 1 perovskite of which we are aware.

The I_2 guests induce small distortions in the Pb−I framework, but these distortions increase octahedral torsion and deviation of the Pb−(μ-I)−Pb bond angle from linearity, which typically increases the bandgap instead of decreasing it.[56,64,65] We turned to electronic structure calculations to determine whether quantum or dielectric confinement is primarily mitigated by I_2 intercalation. Although intercalation causes several new sets of molecular-I_2-derived bands to appear, the I_2 molecules do not appear to mix electronically with the inorganic layers to a significant extent. The I_2-intercalated perovskite $(IC_6)_2[PbI_4]\cdot 2I_2$ instead can be considered a weakly

DOI: 10.1021/acs.chemmater.6b05395
Chem. Mater. 2017, 29, 1868−1884

coupled composite system. Additionally, the bands close to the conduction and valence band edges exhibit negligible dispersion perpendicular to the inorganic layers, so quantum confinement is not significantly reduced compared to $(IC_6)_2[PbI_4]$. We then calculated the spatially resolved high-frequency dielectric constant for slabs of $(IC_6)_2[PbI_4]$ and $(IC_6)_2[PbI_4]\cdot 2I_2$ ($\varepsilon_{\perp,\infty}$, Figure 4B,C) along the direction perpendicular to the inorganic sheets. The $\varepsilon_{\perp,\infty}$ profiles change significantly upon I_2 intercalation. In $(IC_6)_2[PbI_4]$, the average $\varepsilon_{\perp,\infty}$ of the organic layers is low, whereas the $\varepsilon_{\perp,\infty}$ of the inorganic components is much higher. Iodine intercalation completely inverts this dielectric profile such that the regions of highest $\varepsilon_{\perp,\infty}$ now reside inside the organic layers. This improves the ability of the organic layer to screen the excitons in the inorganic layer, substantially decreasing the effects of dielectric confinement and thereby reducing E_b. Therefore, increasing the dielectric constant of the organic layers, through intercalation or covalent attachment of polarizable groups, can significantly decrease the electronic confinement of 2D perovskites.

Careful engineering of the dielectric landscape in perovskites should be a major goal for expanding the range of optical and electronic properties these materials can display. Increasing the dielectric constant of the organic layers in 2D perovskites provides a powerful method for accessing photophysical properties more similar to their 3D analogs, while preserving the greater stability and tunability of the layered organic–inorganic architecture. We postulate that this strategy for reducing the dielectric confinement of 2D perovskites will have even greater effect on their optical and electronic properties when combined with other synthetic strategies, such as reducing quantum confinement by increasing the thickness of the inorganic sheets[12] (described in Section 1.2). Methods for more permanently attaching the polarizable groups to the organic layers should also be developed to impart greater stability to these low-E_b materials.

2.3. Electrochemical Ion Intercalation. The success with neutral-molecule intercalation suggests that electrochemical methods could be used to intercalate charged ions into the organic layers, while electrons are injected into or out of the inorganic sheets to provide charge compensation. These electrochemical methods require that the perovskite contains redox-active centers and a route for ion (de)insertion to balance charge. Such redox-active centers can be envisioned in either the inorganic or organic components, or both.

Reversible ion insertion invokes applications in electrochemical energy storage. Indeed, the lamellar architectures of 2D perovskites are reminiscent of Li or Li-ion battery electrodes such as graphite and $LiCoO_2$.[66] However, we are not aware of explorations of electrochemical ion insertion into hybrid perovskites prior to our investigation using (EDBE)-$[CuCl_4]$ (EDBE = 2,2′-(ethylenedioxy)bis(ethylammonium), Figure 5A).[67] We achieved stable Li^+ cycling in this redox-active Cu^{II}–Cl perovskite containing organic layers composed of diether functionalities. The flexible ether chains were included to mimic the Li^+ binding sites found in typical ethereal battery electrolytes. This yields an organic–inorganic hybrid consisting of a repeating electrode–electrolyte structure. Lithium insertion was deduced by comparing cyclic voltammograms (CVs) of (EDBE)$[CuCl_4]$ in both Li^+ and Bu_4N^+ electrolytes (Figure 5B). The bulky Bu_4N^+ should not insert into the material and thus the CV only shows capacitive charging. We therefore attribute the significant current enhancement observed in the Li^+ electrolyte to Faradaic processes accompanied by Li^+ insertion. Our results are consistent with two possible mechanisms: (1) a conversion reaction (where the perovskite lattice is not preserved) stabilized by atomic-scale integration of organic and inorganic components or (2) an intercalation reaction (where the perovskite structure is preserved). Ex situ PXRD data suggest that the original structure is at least partially recovered upon oxidation and Li^+ removal. Importantly, control studies show that $CuCl_2$ alone or even a mixture of the organic and inorganic components ((EDBE)Cl_2 and $CuCl_2$) do not cycle as a competent Li electrode (Figure 5C). This highlights the advantages of the atomic-level integration of organic and inorganic components afforded by the layered perovskite structure.

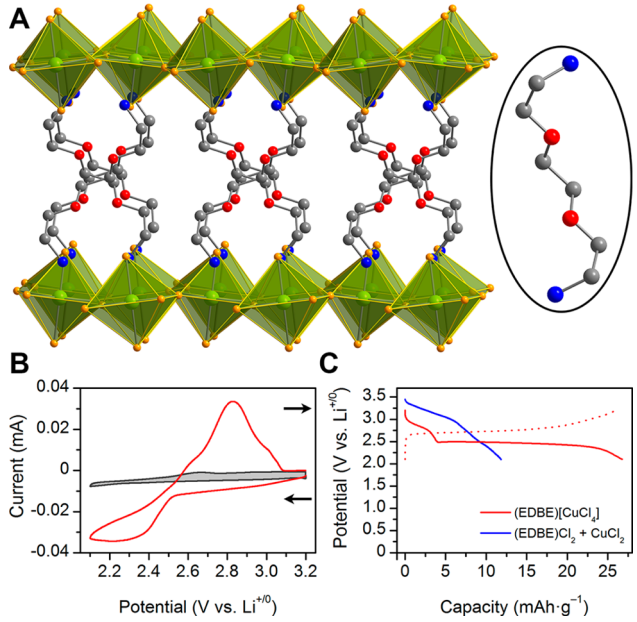

Figure 5. (A) X-ray crystal structure of (EDBE)$[CuCl_4]$. (Inset) EDBE cation. Light green, orange, red, blue, and gray spheres represent Cu, Cl, O, N, and C atoms, respectively. Hydrogen atoms omitted for clarity. (B) Cyclic voltammograms (CVs) of (EDBE)-$[CuCl_4]$ on a carbon electrode in Li^+ (red) and Bu_4N^+ (gray) electrolytes. (C) Discharge (solid line) and charge (dashed line) profiles in a Li battery for (EDBE)$[CuCl_4]$ (red), displaying good voltage and Coulombic efficiency. The irreversible discharge profile for a mixture of the perovskite's constituents is shown for comparison (blue). Adapted from ref 67. Copyright 2014 American Chemical Society.

We demonstrated that this hybrid material can be cycled as a positive electrode (cathode during discharge) in a Li battery (Figure 5C) over 200 times without significant loss in capacity, providing an open-circuit voltage of 3.2 V and a stable discharge voltage of 2.5 V. We obtained an average gravimetric capacity of 26(4) $mA\cdot h\cdot g^{-1}$ at 22 °C, which should be further improved for applications, possibly through metal substitution. This type of inexpensive electrode is suited for grid-scale energy storage, where cost, safety, and lifetime take precedence over gravimetric capacity.

A recent report claims electrochemical ion insertion in the 3D hybrid perovskites (MA)$[PbX_3]$ (X = Br^- or I^-) when operating at voltages relevant for use as a negative electrode (anode during discharge) in a Li-ion battery.[68] However, the lithiated products are not sufficiently structurally or electrochemically characterized to indicate lithium cycling and their reported experimental capacities exceed the theoretical capacity

DOI: 10.1021/acs.chemmater.6b05395
Chem. Mater. 2017, 29, 1868–1884

for a 2 e^- reduction of each lead site, which requires further explanation. Ion insertion appears unlikely in 3D perovskites without dramatic structural rearrangements and conversion reactions are more likely.

Layered hybrid perovskites afford organic and inorganic layers with distinctly different structures, which can be independently optimized for electrochemical energy storage. Here, flexible organic groups with binding sites and/or structures that induce slight porosity can be chosen to facilitate the rapid ion diffusion required for fast charge/discharge rates. Meanwhile, the metal ions in the dense inorganic layers can be chosen to produce high voltages and/or to store multiple electrons per metal site. Similar electrochemical methods could also be used to lightly oxidize or reduce the inorganic layers, thereby doping these semiconductors. We also note that the significant halide mobility in 3D hybrid perovskites[69] may be exploited for ion insertion even in the inorganic framework.

3. SMALL-MOLECULE REACTIVITY

3.1. Organic Layers. The organic layers of 2D hybrid perovskites present many opportunities to impart new chemical reactivity. The confined, close-packed space within the perovskite layers provides an environment that is unique from the solvated environment found in solution-state organic reactions. Therefore, factors that dictate reaction intermediates and regio- and stereoselectivity may vary enough to yield novel products. The inorganic framework can also be used to arrange organic molecules such that intermolecular coupling reactions are favored. In the following sections, we discuss how these features can be exploited to perform chemical reactions within the organic layers of these crystalline solids.

3.1.1. Solid-State Templates: Alkene Polymerization. Postsynthetic polymerization within the organic layers of hybrid perovskites provides a strategy for obtaining both new perovskites and new organic materials. Tieke and co-workers provided the earliest reports of attempts at polymerization within perovskites.[19,70,71] They explored a range of chloride-based perovskites containing Cd^{2+}, Mn^{2+}, and Cu^{2+}. Their best-studied model compound was a Cd−Cl perovskite containing (2*E*,4*E*)-6-aminohexa-2,4-dienoic acid (hereafter denoted as dieneA). Reaction of $(dieneA)_2CdCl_4$ with ultraviolet (UV) light or gamma (γ) radiation yields an extended chain of 1,4-polybutadiene (hereafter $(polydieneA)_{1/m}$, m = polymer chain length) in the organic layer of the perovskite $(polydieneA)_{2/m}[CdCl_4]$ (Figure 6). The polymer propagates along one of the directions defined by the Cd−(μ-Cl)−Cd bonds.[70] The inorganic lattice displays an 8% contraction along this direction upon polymerization, whereas the other in-plane direction in the perovskite shows no change. This contraction of the inorganic sheet stabilizes a compact polymer within the perovskite. The authors attribute the stereoregularity of the polymer to templating effects of the rigid inorganic framework as well as the hydrogen bonding between the carboxylic acid groups.[71] Importantly, UV-light mediated photoreaction of similar butadiene molecules in the solid state (but not within a perovskite) yields only cyclodimers,[72] dimers,[73] or small oligomers.[73] To evaluate the importance of the intermonomer spacing for polymerization, as dictated by the Cd−Cl sheets, the authors also explored the same reaction in a Cu−Cl perovskite.[71] Here, the first-order Jahn−Teller distortion of the d^9 Cu^{2+} centers templates a different packing geometry of the organic cations that disfavors solid-state polymerization, and hence no reactivity was observed.[71]

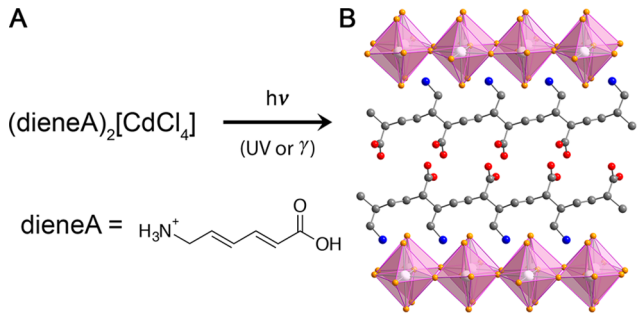

Figure 6. Reaction scheme for photopolymerization of the organic layer of the perovskite (A) $(dieneA)_2[CdCl_4]$. (B) Single crystal X-ray structure of the reaction product: $(polydieneA)_{2/m}[CdCl_4]$.[70] White, orange, red, blue, and gray spheres represent Cd, Cl, O, N, and C atoms, respectively.

Premade polymers have also been incorporated into perovskites. A series of layered Pb−I perovskites containing polyethylenimine (PEI, $M_w \sim 800$ g·mol^{-1}) was recently reported, where the polymer interacts with the inorganic layer at multiple sites through terminal alkylammonium groups.[74] Although the authors were unable to confirm the structure through single-crystal X-ray diffraction, PXRD and optical data were used to assign the layered perovskite structure.

Postsynthetic polymerization within perovskites allows for the stereo- and regioselectivity of the polymerization to be controlled by the inorganic template, which can result in unique polymers. One specific target could be the creation of 2D polymer sheets, reminiscent of covalent organic frameworks (COFs). Incorporating self-healing polymers could impart increased mechanical stability to perovskites employed in applications requiring high durability and long device lifetime. Uniting the field of polymer chemistry with that of crystalline inorganic solids can afford hybrids with new physical properties such as solar-cell absorbers or phosphors with improved tensile strength and flexibility.

3.1.2. Nonporous Sorbents: Radioactive I_2 Capture. Most sorbents designed for small-molecule capture are porous materials such as zeolites and metal−organic frameworks. Here, small molecules typically interact with the pore walls of the sorbent through weak physisorption forces, although placement of coordinatively unsaturated metals[75] and pendant binding groups[76] have allowed for stronger interactions between the guest molecules and the host. In contrast, hybrid perovskites exhibit no appreciable porosity.[17] Despite this lack of space for small-molecule entry, prior studies on small-molecule intercalation into 2D perovskites[18,51] prompted us to expose hybrid perovskites with reactive groups to small-molecule substrates. This afforded the first examples of covalent bond formation (chemisorption) between small molecules and hybrid perovskites.

We synthesized a series of perovskites containing terminal alkene and alkyne groups to exploit the well-known reactivity of halogens with unsaturated hydrocarbons.[77] When exposed to I_2 gas, the perovskite $(HC{\equiv}C(CH_2)_2NH_3)_2[PbBr_4]$ (hereafter $(BYA)_2[PbBr_4]$) undergoes a 36% increase in unit-cell volume to form the perovskite $(HIC{=}CI(CH_2)_2NH_3)_2[PbBr_4]$ (hereafter $(BYA\text{-}I_2)_2[PbBr_4]$, Figure 7).[17] This vapor−solid reaction proceeds topotactically and preserves the crystalline layered perovskite structure, despite the significant rearrangements in the organic layer. The formation of covalent bonds between the

DOI: 10.1021/acs.chemmater.6b05395
Chem. Mater. 2017, 29, 1868−1884

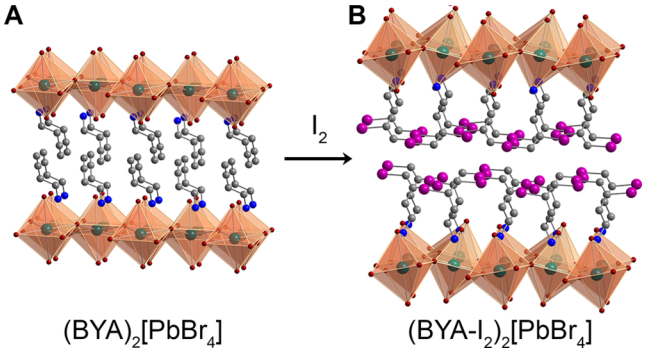

Figure 7. X-ray crystal structures of (A) $(BYA)_2[PbBr_4]$ and (B) its reaction product with I_2: $(BYA\text{-}I_2)_2[PbBr_4]$. Dark green, purple, brown, blue, and gray spheres represent Pb, I, Br, N, and C atoms, respectively. Hydrogen atoms omitted for clarity. Adapted from ref 17 with permission. Copyright 2014 John Wiley and Sons.

perovskite and iodine led us to examine the material's utility in radioactive I_2 capture and containment.

Nuclear power plant waste streams emit gaseous radioactive I_2 isotopes such as ^{129}I, which emits both β and γ radiation with a half-life of 10 million years.[78,79] Solid sorbents such as silver-impregnated zeolites and metal−organic frameworks are being considered to contain these gases from the atmosphere. However, current sorbents are either difficult to produce in large scale or are deactivated by other components in the waste stream such as water vapor and NO_x gases.[80,81] Solid $(BYA\text{-}I_2)_2[PbBr_4]$ shows a gravimetric capacity for I_2 of 43 wt %, which compares well with those of the highest-performing porous sorbents evaluated for I_2 capture.[80,82] Importantly, the nonporous perovskite's volumetric capacity for I_2 capture (1.48 $g{\cdot}cm^{-3}$) exceeds that of the porous sorbents that have unused internal space. Volumetric capacity is more important than gravimetric capacity for these applications because burying the sorbent is currently the most viable long-term disposal strategy. Evaluating $(BYA)_2[PbBr_4]$ for radioactive I_2 capture highlights the power of the organic−inorganic hybrid. Although the organic component alone is hygroscopic and quickly decomposes in solutions containing NO_x, it is stabilized in the perovskite. The perovskite $(BYA)_2[PbBr_4]$ is moisture-stable, and exposure to a gas stream containing 390 ppm I_2 and 1% NO_2 resulted in only a moderate (ca. 10%) loss in capacity over a 24 h period. Notably, the high electron density of the Pb−Br sheets provides an additional benefit: the dense inorganic layers attenuate the radiation emitted from captured ^{129}I to provide increased radiation protection over other sorbents.

3.1.3. Nonporous Sorbents: Timed Halogen Release. Similar to the reactivity of terminal alkynes, terminal alkenes in the organic layers also react with I_2 to yield vicinal diiodoalkanes. Vicinal diiodoalkanes are unstable in solution.[83] They coexist in solution with I_2 and the corresponding alkene, with the equilibrium favoring the alkene. However, we find that vicinal diiodoalkane functionalities are stabilized in the organic layers of perovskites.[17] For example, compared to their solution-state lifetimes, vicinal diiodoalkanes are ca. 100 times more stable in the perovskite $(H_2IC{-}CIH\text{-}(CH_2)_2NH_3)_2[PbBr_4]$ (hereafter $(BEA\text{-}I_2)_2[PbBr_4]$; Figure 8B) with a half-life for I_2 release of 72 h at 25 °C.[17] We attributed the increased stability of the vicinal diiodoalkane in the perovskite to I···I interactions between neighboring diiodoalkane molecules. The length of the alkyl group also

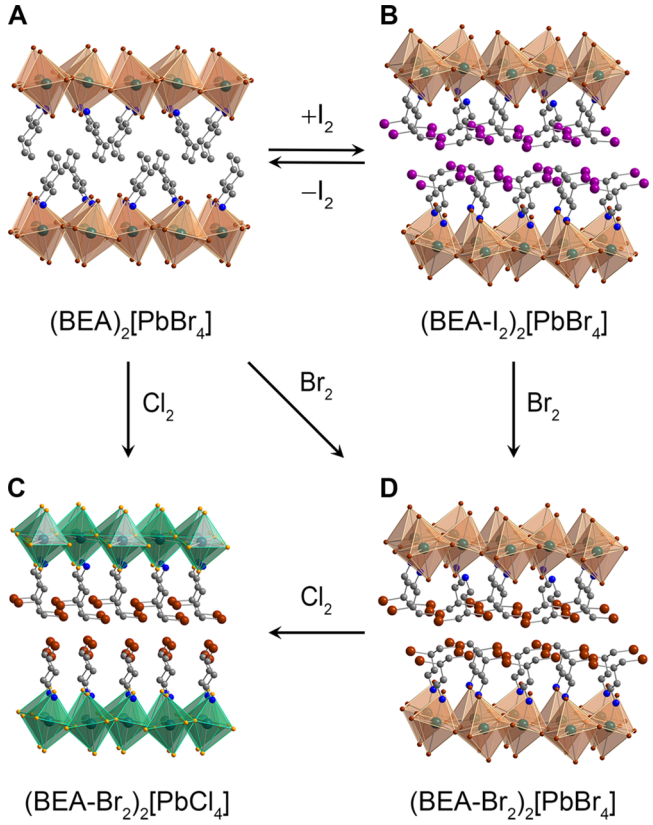

Figure 8. Schematic of postsynthetic reactivity of $(BEA)_2[PbBr_4]$[17] and related perovskites.[17,84] Dark green, purple, brown, orange, blue, and gray spheres represent Pb, I, Br, Cl, N, and C atoms, respectively. Disordered atoms and hydrogens omitted for clarity.

affects the diiodoalkane stability. The shorter chain length of the organic cation in $(H_2IC{-}CIHCH_2NH_3)_2[PbBr_4]$ affords a half-life for I_2 release of 3.2 h at 25 °C. The greater conformational flexibility of the longer alkyl chains may afford better packing that maximizes I···I interactions. Importantly, we can tune the half-life for I_2 release by varying the organic cation, allowing for timed-release of I_2 and inexpensive regeneration of the sorbent.

3.1.4. Nonporous Sorbents: Halogen Separation. Although vicinal diiodoalkanes are unstable to I_2 release under ambient conditions, vicinal dibromoalkanes are stable in solution and the solid state. Exposing $(H_2C{=}CH(CH_2)_2NH_3)_2[PbBr_4]$ (hereafter $(BEA)_2[PbBr_4]$, Figure 8A) to Br_2 vapor affords the new perovskite $(H_2BrC{-}CBrH(CH_2)_2NH_3)_2[PbBr_4]$ (hereafter $(BEA\text{-}Br_2)_2[PbBr_4]$, Figure 8D). The reversibility of I_2 capture and the irreversibility of Br_2 capture allow us to use alkene perovskites to scrub Br_2 from $I_2/Br_2/IBr$ mixtures.[84] As the gas mixture is passed through the perovskite, the irreversible adsorption of Br_2 and IBr shifts the composition of the mixture to favor I_2, purifying the gas stream. Current methods of iodine gas purification involve precipitation of iodine as iodide salts, followed by washing and reoxidation.[85] Although iodide is an essential nutrient found in many food products, bromide can be toxic to human health as it competitively inhibits iodide uptake.[86] Selective reversible and irreversible halogen chemisorption in perovskites afford solid sorbents that scrub trace amounts of Br_2, which can contaminate I_2 streams.

DOI: 10.1021/acs.chemmater.6b05395
Chem. Mater. 2017, 29, 1868−1884

These selective sorbents allow us to tune both the thermodynamics and kinetics of small-molecule capture and release through both organic substitution and crystal-packing effects. The organic layers of perovskites can incorporate a large range of functional groups (e.g., amides, nitriles, alcohols) that can expand the postsynthetic reactivity of these materials, while the close-packed environment within the solid may engender new reactivity not accessible in solution. New synthetic strategies should be developed that allow for still more reactive organic groups to be incorporated into these structures. One intriguing example would be the inclusion of a protecting group that can be removed postsynthetically, which could allow for the inclusion of functional groups that are otherwise incompatible with the perovskite synthetic conditions. These dense, nonporous sorbents, which expand with substrate incorporation, are suitable for stationary applications where volumetric capacity is more important than gravimetric capacity.

3.2. Inorganic Layers: Halide Exchange. Because the valence-band maxima of both 2D and 3D perovskites have strong halide p-orbital character, varying and mixing the halide provides fine control over the materials' bandgap and carrier mobility. Therefore, the chloride, bromide, and iodide analogs of a given perovskite can span a range of optical and electronic properties required for various technologies. For many of these applications, film quality is as important as film composition. Although substituting the halide in the precursor solution is a convenient method for depositing films with different halides, the resulting film morphology differs greatly with the halide. Importantly, we find that postsynthetic halide conversion allows for the morphology of the parent film to be retained in the product. We also show cases where postsynthetic halide exchange affords new perovskites that cannot be formed through traditional solution-state routes.

3.2.1. Redox-Mediated Halide Exchange: 2D Perovskites. Continuing our studies of I_2 and Br_2 addition in alkene perovskites (Sections 3.1.3 and 3.1.4), we explored the effects of Cl_2 addition to the alkene perovskite $(BEA)_2[PbBr_4]$.[84] In contrast to the reactions with I_2 and Br_2, however, reaction of solid $(BEA)_2[PbBr_4]$ with Cl_2 gas does not produce the dichloroalkane perovskite $(BEA\text{-}Cl_2)_2[PbBr_4]$. Instead, mass spectrometry analysis revealed that the organic product contained dibromoalkanes and PXRD analysis suggested a smaller Pb−Cl lattice. Indeed, the Cl_2 is incorporated into the inorganic sheets as chloride anions, and the bromide from the inorganic sheets moves to the organic layers to afford the perovskite $(BEA\text{-}Br_2)_2[PbCl_4]$ (Figure 8C). Surprisingly, the product perovskite remains crystalline despite this massive atomic rearrangement that involves atoms moving across the organic−inorganic interfaces.

To understand this unusual result, we first independently synthesized $(BEA\text{-}Cl_2)_2[PbBr_4]$ through reaction of $(BEA\text{-}Cl_2)$Br and $PbBr_2$, confirming it is a stable, isolable material. Despite this stability, postsynthetic exposure to Cl_2 oxidizes the Pb−Br inorganic sheets instead of oxidizing the alkenes. Additionally, unsaturated organic groups are not required for this reaction; Cl_2 reacts with the bromide perovskite $(BEA\text{-}Br_2)_2[PbBr_4]$ to yield the chloride perovskite $(BEA\text{-}Br_2)_2[PbCl_4]$. We therefore attribute this reactivity to the redox activity of the halogens. Molecular I_2, Br_2, and Cl_2 have standard reduction potentials of 0.54, 1.07, and 1.36 V vs SHE, respectively.[87] Therefore, Cl_2 can oxidize the Br^- ions in the inorganic lattice to form Br_2. The resulting Cl^- ions replace the displaced bromides in the inorganic lattice of the perovskite and the resulting Br_2 adds across the double bonds in the organic layers to form vicinal dibromoalkanes. Here, formation of the organochlorine product is likely suppressed due to the kinetics of competing reactions. Alkene chlorination occurs more slowly than bromination in solution[88−90] and the chloronium intermediate is less stable than the bromonium intermediate, according to computational studies.[91−93] The perovskite $(BEA)_2[PbBr_4]$ provides a model compound for postsynthetic reactivity with halogen gas. A summary of the transformations we have explored with this material and halogens is provided in Figure 8.

To increase our understanding of halogen-mediated reactivity, we also explored how Br_2 reacts with $(IC_6)_2[PbI_4]$, which contains both organic and inorganic iodides. Excess Br_2 oxidizes both the inorganic layers and the alkyl iodide groups to form alkyl bromides in the new perovskite $(BrC_6H_{12}NH_3)_2[PbBr_4]$ (Figure 9C).[52] A few examples of solution-state halogen reactivity with alkyl halides can be found.[94,95] To further parse the kinetics of this reaction, we then considered the stoichiometric reaction between $(IC_6)_2[PbI_4]$ and Br_2 in a 1:2 molar ratio. Here, we form the new perovskite $(IC_6)_2[PbBr_4]$ in 95% yield (Figure 9A). This reactivity suggests that inorganic halide exchange precedes organohalogen exchange in the organic layers and expands our toolbox of postsynthetic reactions to produce new perovskites that cannot be formed in solution. This perovskite is inaccessible by traditional solution-state techniques because bromide displaces the labile organoiodines in solution to form organobromines.

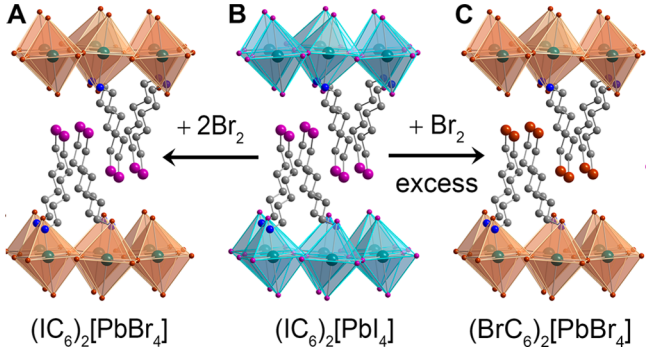

Figure 9. Schematic of perovskite reaction products obtained by exposing (B) $(IC_6)_2[PbI_4]$ to (A) stoichiometric and (C) excess Br_2. Dark green, purple, brown, blue, and gray spheres represent Pb, I, Br, N, and C atoms, respectively. Disordered atoms and hydrogens omitted for clarity. Adapted from ref 52 with permission. Copyright 2016 Royal Society of Chemistry.

3.2.2. Redox-Mediated Halide Exchange: 3D Perovskites. The 3D perovskites $(MA)[PbI_3]$, $(MA)[PbBr_3]$, and $(MA)[PbCl_3]$ have E_g values of 1.6, 2.3, and 2.9 eV, respectively.[96] The Pb−I perovskites exhibit the narrow bandgaps required for single-junction solar-cell absorbers.[97] The higher-bandgap Pb−Br perovskites are candidates as top absorbers in tandem solar cells[98] and both Pb−Br and Pb−Cl perovskites have been used as emitters in optoelectronic devices such as light-emitting diodes[35,99] and lasers.[32,33]

These target technologies require high-quality thin films with uniform coverage. Although many methods have been developed and optimized for depositing high-quality films of the Pb−I perovskites, similar processing does not afford high-

DOI: 10.1021/acs.chemmater.6b05395
Chem. Mater. 2017, 29, 1868−1884

coverage films of Pb−Br or Pb−Cl perovskites. The PbI_2 precursor to the Pb−I perovskite is a 2D material, which may template a more uniform coverage of the substrate. In contrast, $PbBr_2$ and $PbCl_2$ are not layered structures, which may be the cause for greater difficulty in achieving high-coverage films of the Pb−Br and Pb−Cl perovskites. Thin films of $(MA)[PbBr_3]$ formed through simple spin-coating techniques are discontinuous, inhibiting short-circuit current and overall device performance.[98] Using (MA)Cl as a precursor[100] or adding HBr to the spinning solution[101] has been shown to help reduce pinhole formation significantly. However, a method to simply convert Pb−I perovskite films to films of the other halide perovskites would allow us to build on the considerable efforts that have led to the formation of uniform Pb−I perovskite films on various different substrates.

As discussed in Section 3.2.1, the reduction potentials of the halogens predispose bromide to oxidation by Cl_2 and iodide to oxidation by either Br_2 or Cl_2. We reasoned that the reactivity we first observed in 2D perovskites could easily be extended to 3D perovskites. Upon reaction with Br_2 or Cl_2 vapor, dark red-brown $(MA)[PbI_3]$ films convert to orange or colorless films, respectively (Figure 10).[84] Similarly, orange $(MA)[PbBr_3]$ films become colorless upon exposure to Cl_2. When concentrated vapor is used, the conversion occurs in seconds. However, when the halogen vapor is diluted, the reaction slows down significantly affording higher-quality films. PXRD analysis of the products confirms that $(MA)[PbBr_3]$ and $(MA)[PbCl_3]$ are formed through reaction with Br_2 and Cl_2, respectively. Scanning electron microscopy micrographs of typical films before and after the reaction were collected to assess the conversion's effect on film quality (Figure 11). The parent $(MA)[PbI_3]$ films completely cover the substrate. Importantly, this high coverage is retained in the product films of $(MA)[PbBr_3]$ and $(MA)[PbCl_3]$. In contrast, when the bromide or chloride precursors are used to form the corresponding $(MA)[PbBr_3]$ or $(MA)[PbCl_3]$ films (PbX_2 + (MA)X where X = Cl^- or Br^-) by spin coating, large gaps between the grains of the films can be seen (Figure 11B and C insets). Therefore, the parent $(MA)[PbI_3]$ film templates the formation of high-quality bromide or chloride perovskite films. Importantly, this conversion produces only gaseous byproducts and no purification or annealing steps are required.

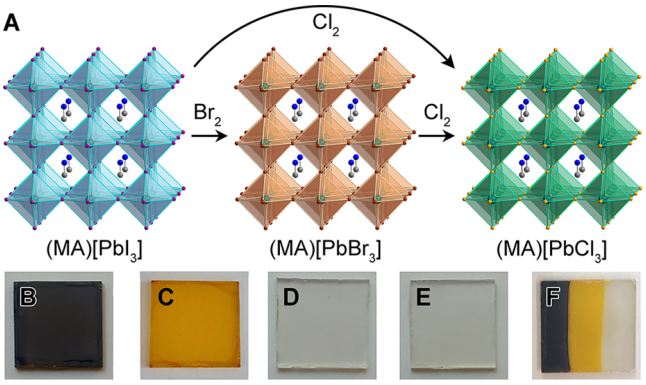

Figure 10. (A) Schematic of the reaction of $(MA)[PbX_3]$ (X = I^- and Br^-) with Br_2 or Cl_2 gas. Dark green, purple, brown, orange, blue, and gray spheres represent Pb, I, Br, Cl, N, and C atoms, respectively. Hydrogen atoms omitted for clarity. Photographs of (B) a $(MA)[PbI_3]$ film, (C) a $(MA)[PbBr_3]$ film prepared by exposing a $(MA)[PbI_3]$ film to Br_2, (D) a $(MA)[PbCl_3]$ film prepared by sequentially exposing a $(MA)[PbI_3]$ film to Br_2 and Cl_2, and (E) a $(MA)[PbCl_3]$ film prepared by exposing a $(MA)[PbI_3]$ film to Cl_2. (F) Film of all three perovskites formed by exposing parts of a $(MA)[PbI_3]$ film to Br_2 and then to Cl_2 using a mask. Adapted from ref 84 with permission. Copyright 2015 Royal Society of Chemistry.

After assessing the advantages of postsynthetic halide conversion in halide perovskites through reaction with halogen gas, we further proposed that partial halide conversion provides a halide compositional gradient in the film extending from the surface to the interior. Such a gradient will lead to a sloping valence-band maximum that may be used for shuttling charge carriers toward their respective current collectors.[84] One report has since demonstrated such a compositional halide gradient in fabricated devices through postsynthetic conversion of the surface of $(MA)[PbI_3]$ films.[102] Here, enhanced hole extraction and an increase in the open-circuit voltage resulted in an increase in overall device efficiency. However, the bromide/iodide halide gradient was unstable to device operating conditions.[102] Light-mediated halide segregation, an effect we observed in mixed-halide perovskite films,[103] likely facilitates the homogenization of the halide gradient. Other reports have shown that interconversion between $(MA)[PbCl_3]$, $(MA)[PbBr_3]$, and $(MA)[PbI_3]$ can be achieved by exposing them to the desired (MA)X salt (X = Cl^-, Br^-, or I^-) in the vapor[104] or solution[105] phase. This form of ion exchange mimics cation exchange in ionic nanocrystals.[8] Similar to the reaction with (MA)X salts, a recent report has shown halide exchange in 3D perovskites through exposure to gaseous hydrohalic acids.[106] The authors were able to obtain single-crystal X-ray diffraction structures from the converted crystals, indicating that the

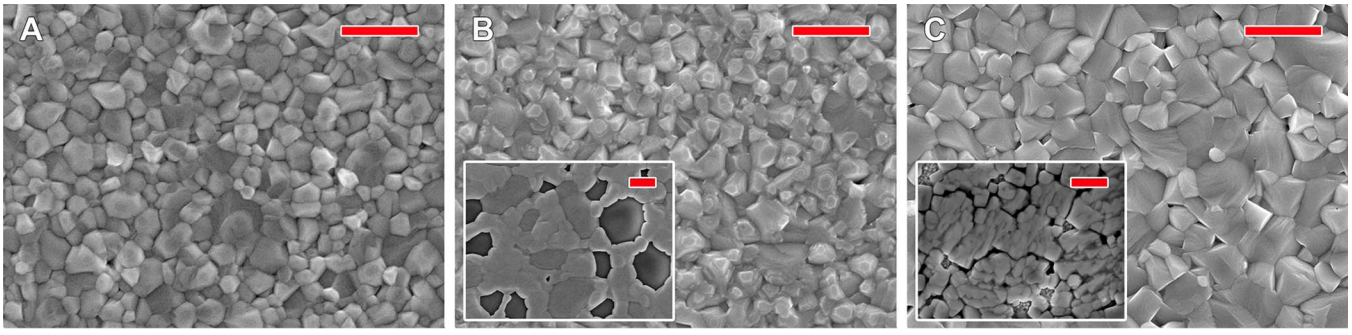

Figure 11. Scanning electron micrographs of (A) a $(MA)[PbI_3]$ film, (B) a $(MA)[PbBr_3]$ film formed by exposing a $(MA)[PbI_3]$ film to Br_2 gas, and (C) a $(MA)[PbCl_3]$ film formed by exposing a $(MA)[PbI_3]$ film to Cl_2 gas. Insets depict films independently fabricated using PbX_2 and (MA)X (X = Cl^- or Br^-) in isopropyl alcohol. All scale bars denote 1 μm. Adapted from ref 84 with permission. Copyright 2015 Royal Society of Chemistry.

DOI: 10.1021/acs.chemmater.6b05395
Chem. Mater. 2017, 29, 1868−1884

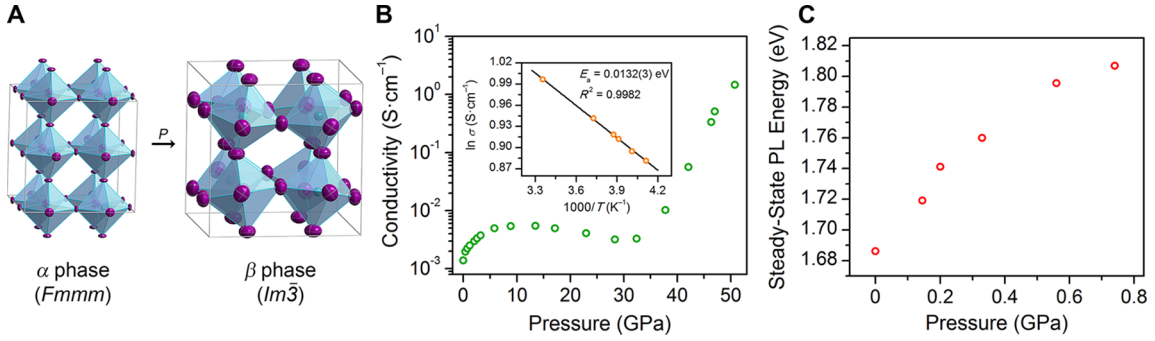

Figure 12. High-pressure properties of $(MA)[PbI_3]$. (A) Single-crystal X-ray structures at ambient pressure (α phase) and 0.7 GPa (β phase). Dark green and purple spheres represent Pb and I atoms, respectively. Disordered atoms and organic groups are omitted. (B) Conductivity with increasing pressure. (Inset) Arrhenius fit of the temperature dependence of conductivity at 51 GPa, yielding an activation energy (E_a) of 13.2(3) meV. (C) Steady-state PL energy during or immediately after light-soaking $(MA)[Pb(Br_{0.6}I_{0.4})_3]$ as a function of pressure within its α phase. Adapted from ref 120. Copyright 2016 American Chemical Society.

reactions proceeded as single-crystal-to-single-crystal transformations.

Our work on I_2 intercalation[52] suggests that intercalation precedes halogen-mediated reactivity in 2D perovskites. However, 3D perovskites and 2D perovskites with organic monolayers[52] are not conducive to small-molecule intercalation. Therefore, the reaction propagation mechanism in these nonporous structures remains to be fully understood. Two likely candidates are (1) surface reaction propagated by the inherent halide mobility of halide perovskites or (2) halogen incorporation (with substantial structural rearrangement) followed by reaction. Although we can perform these reactions under rigorously anhydrous conditions, we cannot eliminate the possibility of very slight dissolution and reprecipitation aided by trace moisture. Even in this case, the different products we isolate in the solid-state reactions versus those obtained from solution-state reactions indicate that the parent solid still templates the product in some manner.

Others have recently shown that small molecules can incorporate into perovskites and disrupt their structure. For example, NH_3[107] and CH_3NH_2[108] were reported to incorporate into $(MA)[PbI_3]$ causing the dark brown/black perovskite to become light yellow in color. Interestingly, this process is reversible in both cases; when the material is removed from the guest-molecule atmosphere, the original perovskite phase reforms. Methylamine intercalation into PbI_2 has also been recently used to form a precursor for $(MA)[PbI_3]$ films.[109] Further exploration into small-molecule-mediated intercalation or conversion reactions in hybrid perovskites should allow us still better control over expanding their accessible compositions, structures, and morphologies.

The redox-mediated halide substitution reactions in both the organic and inorganic layers that we developed should be extended to other redox-active small molecules. For example, pseudohalides could partially substitute for halides in the lattice to induce steric strain or chemical pressure, and thereby tune the perovskite's optoelectronic properties (see Section 4 for more details). Such postsynthetic reactions, which use the parent lattice as a template, could yield strained architectures that are typically disfavored during standard solution-state self-assembly reactions.

4. PRESSURE RESPONSE

Pressure can induce dramatic effects in solids,[110,111] yet it remains an underutilized tool for manipulating the properties of materials. Similar to the postsynthetic transformations discussed above, during material compression the parent structure guides the resulting architecture, while pressure application affords wholly new properties. Diamond-anvil cells (DACs) access pressures on the gigapascal (GPa) scale and allow for a variety of in situ physical, spectroscopic, and diffractive characterization techniques. By subjecting these crystalline hybrids to elevated pressures, we can understand the relationship between compression-induced structural and electronic changes. This provides a deeper understanding of how the material responds to compression and also directs the design of new hybrids that show targeted properties. For example, theoretical frameworks have been developed that relate chemical pressure (steric effects) to mechanical pressure,[112] indicating that lattice strain induced by ion substitution or intercalation could mimic the effects of mechanical compression. In the following sections, we discuss the pressure-induced structural and electronic evolution of both 3D and 2D hybrid perovskites.

4.1. 3D Perovskites. The pressure response of 3D hybrid perovskites' electronic structures is of particular interest owing to their promise for optoelectronic applications. Though their pressure−temperature phase relations were examined decades ago,[113,114] the pressure-induced effects of 3D hybrid perovskites remained relatively unexplored until recently. A structural study examined $(MA\text{-}d_6)[PbBr_3]$ ($MA\text{-}d_6 = CD_3ND_3^+$) up to ca. 2.8 GPa using neutron diffraction.[115] This complements an earlier PL study of $(MA)[PbBr_3]$ up to ca. 5 GPa.[116] The structures of the analogous Sn−I perovskites were also analyzed under pressures up to just above 4 GPa using PXRD.[117] Recent efforts have also aimed to study the electronic properties of perovskites under pressure; the pressure-dependent resistivity of both bulk $(MA)[PbBr_3]$[118] and $(MA)[PbI_3]$ nanorods[119] have been reported. Our recent work reported the first high-pressure single-crystal structures of hybrid perovskites, allowing us to precisely track the atomic coordinates of $(MA)[PbX_3]$ ($X = Br^-$ or I^-) as a function of pressure.[120] We combined these structural studies at pressures up to ca. 50 GPa with PL and conductivity measurements, as well as electronic structure calculations to present a comprehensive analysis of the system under pressure. Subsequently, several additional high-pressure studies have been reported on Pb−Br, Pb−I, and Sn−I systems.[121−126] Some of these studies have shown enhancement of optoelectronic properties under pressure, including

DOI: 10.1021/acs.chemmater.6b05395
Chem. Mater. 2017, 29, 1868−1884

prolonged carrier lifetime in (MA)[PbI_3][124] and enhanced photocurrent after compression in (MA)[SnI_3].[126]

These recent studies show that the 3D hybrid perovskites are quite compressible compared to many other crystalline solids. During compression in relatively low-pressure regimes, they exhibit structural phase transitions that correlate with discontinuities in the evolution of their bandgap or PL energies. Indeed, their structures are strongly coupled to their electronic behavior, and even subtle changes to the lattice within a given phase are reflected in their photophysical properties.

When subjected to hydrostatic pressure, the pseudocubic (indexed as tetragonal[127−129] or orthorhombic[120]) α phase of (MA)[PbI_3] undergoes a transition to the cubic $Im\bar{3}$ β phase at ca. 0.3 GPa (Figure 12A),[120,121,125] although some reports have instead claimed an orthorhombic $Imm2$ space group.[122,124] Likewise, (MA)[$PbBr_3$] undergoes a similar transition from cubic $Pm\bar{3}m$ to cubic $Im\bar{3}$ at ca. 0.9 GPa.[115] These α-to-β transitions are accompanied by pronounced interoctahedral tilting, indicated by the Pb−X−Pb angle θ_R. Further volume reduction during compression within a given phase occurs through a combination of decreased θ_R and decreased Pb−X bond length (d). Decreasing d should increase orbital overlap and thereby increase band dispersion and decrease the bandgap. Conversely, octahedral tilting (which decreases θ_R) should decrease orbital overlap and band dispersion and increase E_g. This simple postulate is consistent with the observed PL energy shifts and calculated E_g values from our work,[120] as well as PL and absorption spectroscopy data from other reports.[121,124,125] Both the iodide and bromide perovskites undergo partial amorphization above ca. 3 GPa, which quenches PL from the materials. Interestingly, this amorphization is fully reversible upon decompression. More structural analysis is required to determine the exact nature of the amorphization. Transport measurements on (MA)[PbI_3] in this γ phase show a dramatic increase in conductivity and a low activation energy for conduction of 13.2(3) meV at 51 GPa (Figure 12B), suggesting the approach of a metallic state.[120]

We also explored the effects of compression on the mixed-halide perovskites (MA)[$Pb(Br_xI_{1-x})_3$] ($0 < x < 1$). The bandgap of these materials can be continuously tuned between that of the pure iodide (1.6 eV) and the pure bromide (2.3 eV), making mixed-iodide/bromide perovskites attractive candidates as the high-bandgap absorber in tandem solar cells. However, high open-circuit voltages have been difficult to achieve in devices employing these materials.[127] We previously found that the perovskites (MA)[$Pb(Br_xI_{1-x})_3$] ($0.2 < x < 1$) are unstable to light.[103] Upon light exposure for a few minutes, their PL energies discretely redshift to a lower-energy value, suggesting the formation of low-energy trap states. Interestingly, this process is reversible, and the original material regenerates in the dark. We proposed that this instability arose from light-induced, reversible halide segregation into bromide-rich and iodide-rich domains. Halide segregation requires halide mobility. We therefore reasoned that a compressed, stiffer lattice may kinetically suppress ion transport. Alternatively, because halide transport in related materials is thought to occur through halide vacancies,[130−132] compression may alter the thermodynamics of halide transport by changing the defect distribution in the lattice. Indeed, compression below 1 GPa can mitigate or completely suppress this light-induced instability.[120] The mixed-halide perovskites show the same α-to-β phase transitions with compression as the pure bromide or iodide perovskites. Although we still observe the PL redshift with increased irradiation time in the α phase, the energy to which the PL band shifts increases with compression, allowing for higher-energy steady-state PL at higher pressures (Figure 12C). Notably, halide segregation appears to be suppressed in the high-pressure β phase. A new PL peak emerges at the onset of the β phase, which does not redshift with illumination time and shifts only as a function of pressure. This work motivates the examination of chemical pressure as a method to obtain higher voltages from solar cells employing mixed-halide perovskite absorbers.

4.2. 2D Perovskites: Cu−Cl Perovskites. Owing in part to their similarity to the cuprate superconductors, whose critical temperature (T_c) varies with increasing pressure,[133,134] the pressure-response of 2D Cu−Cl perovskites has been investigated for decades.[46,135−138] Here, the d^9 Cu(II) centers exhibit a pronounced Jahn−Teller (JT) distortion (Figure 13A). The distorted octahedra within a single inorganic layer

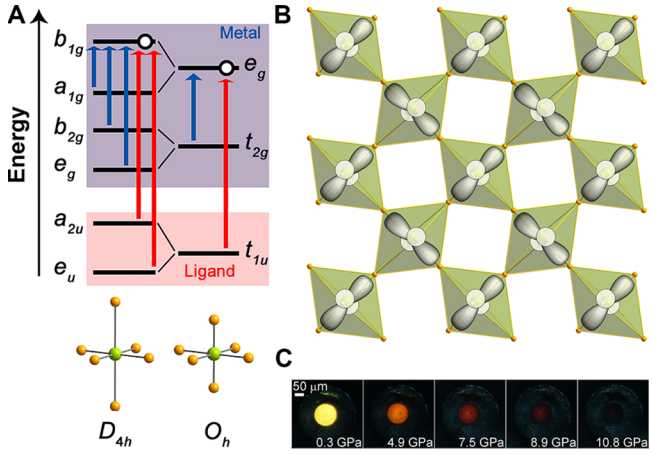

Figure 13. (A) Orbital energy diagram of Cu−Cl octahedra with D_{4h} and O_h symmetry showing possible d−d (blue) and charge-transfer (red) transitions. (B) A single Cu−Cl layer viewed from above, displaying antiferrodistortive alignment of the Jahn−Teller axes. Schematic dx^2-y^2 orbitals are overlaid to illustrate their orthogonality. (C) Optical micrographs of (EDBE)[$CuCl_4$] in a DAC showing piezochromism. Adapted from ref 47. Copyright 2015 American Chemical Society.

align with their elongated axes positioned perpendicular to those of their nearest neighbors (Figure 13B). This antiferrodistortive arrangement results in orthogonality between the partially occupied dx^2-y^2 orbitals of adjacent octahedra (Figure 13B). Although a half-filled band should provide a conduction pathway, the lack of orbital overlap between the partially occupied d orbitals likely contributes to these materials' insulating nature.

Early work attempted to postsynthetically suppress this cooperative JT distortion with pressure,[46,136] which could allow for orbital reordering and the formation of partially occupied electronic bands. A first-order phase transition, accompanied by a piezochromic change from yellow to orange at ca. 4 GPa (Figure 13C),[46,136] was initially thought to indicate suppression of the JT distortion. However, this phase transition was subsequently linked to in-plane rotations (tilting) of the Cu−Cl octahedra,[137,138] and not to significant changes in the Cu coordination sphere. These prior studies only examined the effects of pressures up to ca. 16 GPa, and much higher pressures were considered necessary to suppress the JT

DOI: 10.1021/acs.chemmater.6b05395
Chem. Mater. 2017, 29, 1868−1884

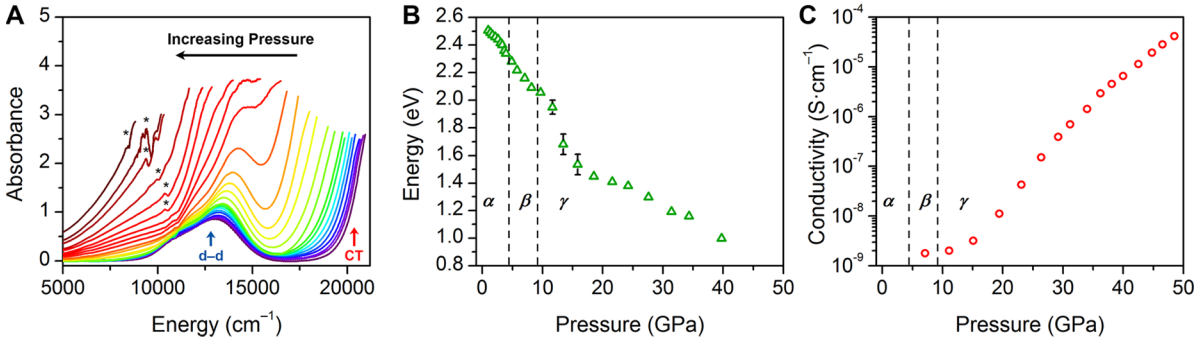

Figure 14. (A) Variable-pressure optical absorption spectra of (EDBE)[$CuCl_4$]. Asterisks indicate a detector change between visible and IR wavelengths. The charge-transfer (CT) edge and d–d transitions are indicated. (B) CT-edge energy as a function of pressure. (C) Electronic conductivity for (EDBE)[$CuCl_4$] as a function of pressure. Adapted from ref 47. Copyright 2015 American Chemical Society.

distortion.[138] We therefore examined the Cu–Cl perovskite (EDBE)[$CuCl_4$] (EDBE = 2,2′-(ethylenedioxy)bis-(ethylammonium)) under pressures up to ca. 60 GPa.[47] At high pressures, we observed unprecedented piezochromism for a Cu–Cl perovskite, from translucent yellow to opaque black, accompanied by dramatic changes in electronic transport, affording the first example of appreciable conductivity in a Cu–Cl perovskite.

By measuring high-pressure PXRD of (EDBE)[$CuCl_4$], we first corroborated the first-order phase transition between α and β phases at ca. 4 GPa reported previously, when the perovskite changes from translucent yellow to translucent orange.[46,135−138] At higher pressures, however, we observed a second-order phase transition to a γ phase indicated by an increase in lattice stiffness above ca. 8 GPa. Intriguingly, the perovskite turns opaque black with compression above this second-order transition. The dominant electronic transition in Cu–Cl perovskites has been assigned as a ligand-to-metal charge transfer (Figure 13A).[135,139] The perovskite's absorption spectra show a distinct redshift of this charge-transfer (CT) band with compression (Figure 14A,B). Furthermore, we measured an increase in electrical conductivity of ca. 5 orders of magnitude up to 50 GPa (Figure 14C). Interestingly, the activation energy for conduction (0.232(1) eV at ca. 40 GPa) is substantially lower than the energy of the CT band (ca. 1 eV) at comparable pressures. This suggests that, above the second phase transition, a combination of octahedral tilting and bond compression at least partially relieves the orthogonality of the d orbitals, providing a new conduction pathway revealed by material compression.

4.3. 2D Perovskites: Pb–I–SCN Perovskites. Early high-pressure studies on the 2D Pb–I perovskite, $(C_4H_9NH_3)_2[PbI_4]$, reported a bandgap decrease with compression, reflected in the material's PL energy. The absorption edge of ca. 2.3 eV was reported to decrease upon compression to ca. 2 eV, albeit at high pressures exceeding 24 GPa.[140] To explore how the perovskite's compressibility could be modified through compositional tuning, we investigated the effects of compression on a related 2D perovskite where the terminal halides were replaced by thiocyanides: $(MA)_2[PbI_2(SCN)_2]$.[16] This material was initially considered to be a promising solar-cell absorber with a low bandgap and high moisture stability. Subsequent work, however, showed that it had a much higher bandgap than previously thought[141] and poor water stability.[142] However, as discussed below, the material has intriguing properties for a 2D perovskite, which can be further modulated through compression.

Solid $(MA)_2[PbI_2(SCN)_2]$ (Figure 15A) has atypically low E_g and E_b values for an n = 1 perovskite.[142] These values are

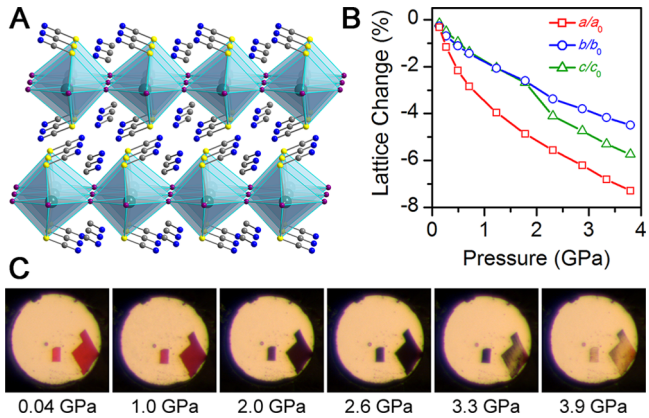

Figure 15. (A) X-ray crystal structure of $(MA)_2[PbI_2(SCN)_2]$.[16] Dark green, purple, yellow, blue, and gray spheres represent Pb, I, S, N, and C atoms, respectively. Hydrogen atoms omitted for clarity. (B) Lattice parameter contraction with compression. (C) Optical micrographs showing the piezochromism of $(MA)_2[PbI_2(SCN)_2]$ single crystals upon compression. Adapted from ref 142. Copyright 2016 American Chemical Society.

intermediate between those for 3D Pb–I perovskites and typical n = 1 Pb–I perovskites. Notably, $(MA)_2[PbI_2(SCN)_2]$ has the shortest interlayer separation of which we are aware for a (100) Pb–I perovskite of 9.2901(9) Å. All Pb and bridging I atoms reside in the same plane, with no out-of-plane octahedral tilting and minimal in-plane octahedral tilting. The short interlayer distance, reduced octahedral tilting in the inorganic sheets, and the covalency of the Pb–S linkages may all contribute to this perovskite's low E_g of 2.33 eV and E_b of 200 meV. We therefore reasoned that pressure could substantially affect its photophysical properties.

The short interlayer spacing and E_g can be further reduced with compression (Figure 15B).[142] The crystallographic a axis (layer stacking direction) shows a monotonic decrease by 7.3% from 0 to 3.8 GPa, whereas the b and c axes contract in a milder fashion. Pronounced discontinuities in the c-axis length and unit-cell volume at 2.3 GPa suggest a phase transition. The material also exhibits dramatic piezochromism, reversibly converting from translucent red to opaque black at 2.6 GPa and then to translucent yellow at 3.9 GPa (Figure 15C). This piezochromism is manifested in the PL spectra of a single crystal of $(MA)_2[PbI_2(SCN)_2]$ as a function of pressure. Upon

DOI: 10.1021/acs.chemmater.6b05395
Chem. Mater. 2017, 29, 1868−1884

compression, the PL redshifts as the single crystals progressively become opaque, followed by a blueshift as the color of the crystals lightens. Assuming no change in Stokes shift of the excitonic emission or of the E_b within this pressure range, we estimate a 0.3 eV decrease in E_g to ca. 2.0 eV at 2.6 GPa as the interlayer distance contracts by 6.0%. The material's black color at 2.6 GPa suggests that the E_g value may be still lower than this estimate. Notably, the pressure required to achieve a ca. 2 eV bandgap in $(MA)_2[PbI_2(SCN)_2]$ is less than the corresponding pressure for $(C_4H_9NH_3)_2[PbI_4]$ by 21 GPa.[140] This demonstrates the substantial role that perovskite composition and structure can play in tuning material compressibility and pressure response.

The pressure-induced transformations discussed above are reversible. However, they help elucidate what effects could be more permanently realized through the application of chemical pressure. For example, the improved light stability reported in mixed-halide perovskites with mixed A-site cations (such as $Cs^+/(NH_2)_2CH^+$)[143] may indeed be a manifestation of the effects of chemical pressure, similar to the mechanically induced changes we observed.[103,144] Dramatic changes to the physical and electronic properties of halide perovskites require pressures in the GPa scale. Designing perovskites with greater pressure response may decrease the pressures required for these transformations to a range that is easier to access in technology.

5. SUMMARY AND OUTLOOK

Postsynthetic transformations of hybrid perovskites provide an opportunity to overcome some synthetic limitations to these important materials. Their optical and electronic versatility, in combination with their synthetic tunability, make them prime candidates for the development of transformations that further expand their functionality. In the above sections, we have provided a condensed summary of current progress in the field. We have concluded each section with our perspective on where the field may head and examples of worthy future targets.

These highly crystalline hybrids provide a forgiving platform for postsynthetic manipulations involving substantial atomic rearrangements. Although some reactions involve individual components of the perovskite, simultaneous reactivity can be achieved across both organic and inorganic components, while the crystalline perovskite structure is retained in the product. External stimuli such as pressure or radiation can also modify the material's structure and photophysical properties. Importantly, the product's crystallinity allows us to track precisely how the structure responds to these perturbations.

The transformations discussed here represent only a small fraction of the potential toolbox of postsynthetic strategies. Early work on 2D perovskites focused on the magnetic[145] and optical[146] properties of the inorganic layers, where simple alkyl ammonium cations in the organic layers served only to insulate the inorganic sheets. In the hands of synthetic chemists, the organic layers have now been functionalized for greater reactivity (e.g., small-molecule capture through both intercalation[18,52] and chemisorption,[17,84] light-induced polymerization,[70] and electrochemical ion cycling[67]) and functionality (e.g., dye molecules in the organic layers facilitating electroluminescence,[14] more polarizable organic layers affording reduced electronic confinement in the inorganic layers,[52] and hydrophobic molecules in the organic layers imparting moisture stability to 2D perovskite solar-cell absorbers[12,49]). The organic layers remain a mostly untapped source of expansion for the synthetic space of hybrid perovskites, and we believe that the inclusion of designer molecules with targeted functionality can greatly expand the number of available postsynthetic transformations. Similarly, the expansion of the inorganic constituents to include more reactive metals and alternative ligands to halides can substantially increase the number of available postsynthetic strategies.

Hybrid perovskites provide an ideal platform for postsynthetic transformations involving the manipulation of ionic and covalent interactions as well as structural deformations. We envision that future developments in this field will bring still richer structural diversity and greater functionality to these materials, which have already proven their technological worth. We hope that this discussion motivates a larger effort toward developing this nascent research field for both fundamental studies and applications in technology.

AUTHOR INFORMATION

Corresponding Author

*H. I. Karunadasa. E-mail: hemamala@stanford.edu.

ORCID

Adam Jaffe: 0000-0002-9886-0249

Hemamala I. Karunadasa: 0000-0003-4949-8068

Notes

The authors declare no competing financial interest.

Biographies

Ian C. Smith is a Ph.D. candidate studying materials and inorganic chemistry under Prof. Hemamala Karunadasa at Stanford University. He graduated magna cum laude from Cornell University, where he double-majored in Chemistry and Mathematics and worked for Prof. Francis DiSalvo. His current research focuses on the synthesis, characterization, and implementation of novel perovskite materials for photovoltaics and other energy applications.

Matthew D. Smith is a Ph.D. candidate in Chemistry in Prof. Hemamala Karunadasa's group at Stanford University. He received his B.S. in Chemistry while working on amine-templated metal oxides for Prof. Alexander Norquist and Prof. Joshua Schrier at Haverford College. His current research interests include the fundamental optoelectronic properties and excited-state carrier dynamics of 2D halide perovskites focusing on potential applications in luminescence.

Adam Jaffe is a Ph.D. candidate in Inorganic Chemistry at Stanford University in the research group of Prof. Hemamala Karunadasa. He received his A.B. in Chemistry summa cum laude from Princeton University in 2012 while working for Prof. Andrew Bocarsly on ethanol electrooxidation in polymer-electrolyte membrane fuel cells. His graduate research focuses on hybrid materials for electrochemical energy storage and solid-state lighting as well as their properties under extreme pressures.

Yu Lin received her B.S. in Earth Sciences from Nanjing University, China in 2007 and Ph.D. in the Department of Geological and Environmental Sciences from Stanford University in 2013. After her postdoctoral research in the Department of Geological Sciences and Department of Chemistry at Stanford from 2013 to 2015, she received an Early Investigator Fellowship and became an associate staff scientist at the Stanford Institute for Materials and Energy Sciences at SLAC in 2016. Her research centers on understanding the behavior of energy-relevant materials under extreme conditions.

Hemamala I. Karunadasa is an assistant professor in Chemistry at Stanford University. She studied geometrically frustrated magnets for her A.B. from Princeton University and molecular catalysts for water splitting for her Ph.D. from the University of California at Berkeley.

DOI: 10.1021/acs.chemmater.6b05395
Chem. Mater. 2017, 29, 1868−1884

She developed electrocatalysts for hydrocarbon oxidation as a postdoctoral researcher at the California Institute of Technology. Her group synthesizes new functional materials with an emphasis on 2D and 3D halide perovskites.

■ ACKNOWLEDGMENTS

This research was funded by the National Science Foundation CAREER award (Grant DMR 1351538), the Alfred P. Sloan Fellowship, and the Global Climate and Energy Project (GCEP). M.D.S. is supported by an NSF Graduate Research Fellowship (DGE-114747). A.J. thanks the Stanford Department of Chemistry for support through the William S. Johnson Fellowship. Y.L. is supported by the Department of Energy, Office of Science, Basic Energy Sciences, Materials Sciences and Engineering Division, under Contract DE-AC02-76SF00515.

■ REFERENCES

(1) Morris, W.; Doonan, C. J.; Furukawa, H.; Banerjee, R.; Yaghi, O. M. Crystals as Molecules: Postsynthesis Covalent Functionalization of Zeolitic Imidazolate Frameworks. *J. Am. Chem. Soc.* **2008**, *130*, 12626−12627.

(2) Bloch, E. D.; Britt, D.; Lee, C.; Doonan, C. J.; Uribe-Romo, F. J.; Furukawa, H.; Long, J. R.; Yaghi, O. M. Metal Insertion in a Microporous Metal−Organic Framework Lined with 2,2′-Bipyridine. *J. Am. Chem. Soc.* **2010**, *132*, 14382−14384.

(3) Aubrey, M. L.; Ameloot, R.; Wiers, B. M.; Long, J. R. Metal-Organic Frameworks as Solid Magnesium Electrolytes. *Energy Environ. Sci.* **2014**, *7*, 667−671.

(4) Brozek, C. K.; Dinca, M. Cation Exchange at the Secondary Building Units of Metal-Organic Frameworks. *Chem. Soc. Rev.* **2014**, *43*, 5456−5467.

(5) Kim, M.; Cahill, J. F.; Su, Y.; Prather, K. A.; Cohen, S. M. Postsynthetic Ligand Exchange as a Route to Functionalization of 'Inert' Metal-Organic Frameworks. *Chem. Sci.* **2012**, *3*, 126−130.

(6) Distefano, G.; Suzuki, H.; Tsujimoto, M.; Isoda, S.; Bracco, S.; Comotti, A.; Sozzani, P.; Uemura, T.; Kitagawa, S. Highly Ordered Alignment of a Vinyl Polymer by Host-Guest Cross-Polymerization. *Nat. Chem.* **2013**, *5*, 335−341.

(7) Wang, Z.; Cohen, S. M. Postsynthetic Modification of Metal-Organic Frameworks. *Chem. Soc. Rev.* **2009**, *38*, 1315−1329.

(8) Son, D. H.; Hughes, S. M.; Yin, Y.; Alivisatos, P. A. Cation Exchange Reactions in Ionic Nanocrystals. *Science* **2004**, *306*, 1009−1012.

(9) Goodenough, J. B. Electronic and Ionic Transport Properties and Other Physical Aspects of Perovskites. *Rep. Prog. Phys.* **2004**, *67*, 1915−1993.

(10) Dohner, E. R.; Hoke, E. T.; Karunadasa, H. I. Self-Assembly of Broadband White-Light Emitters. *J. Am. Chem. Soc.* **2014**, *136*, 1718−1721.

(11) Xu, Z.; Mitzi, D. B.; Dimitrakopoulos, C. D.; Maxcy, K. R. Semiconducting Perovskites $(2\text{-}XC_6H_4C_2H_4NH_3)_2SnI_4$ (X = F, Cl, Br): Steric Interaction Between the Organic and Inorganic Layers. *Inorg. Chem.* **2003**, *42*, 2031−2039.

(12) Smith, I. C.; Hoke, E. T.; Solis-Ibarra, D.; McGehee, M. D.; Karunadasa, H. I. A Layered Hybrid Perovskite Solar-Cell Absorber with Enhanced Moisture Stability. *Angew. Chem., Int. Ed.* **2014**, *53*, 11232−11235.

(13) Depmeier, W. The Uniqueness of the Propyl Compound in the Series $(C_nH_{2n+1}NH_3)_2MnCl_4$ with n = 1−10. *J. Solid State Chem.* **1979**, *29*, 15−26.

(14) Mitzi, D. B.; Chondroudis, K.; Kagan, C. R. Design, Structure, and Optical Properties of Organic−Inorganic Perovskites Containing an Oligothiophene Chromophore. *Inorg. Chem.* **1999**, *38*, 6246−6256.

(15) Yuan, B.-L.; Lan, H.-C.; Chen, Y.-P.; Li, Y.-B. Bis(3-carboxypropanaminium) Tetrachlorocuprate(II). *Acta Crystallogr., Sect. E: Struct. Rep. Online* **2004**, *60*, m617−m619.

(16) Daub, M.; Hillebrecht, H. Synthesis, Single-Crystal Structure and Characterization of $(CH_3NH_3)_2Pb(SCN)_2I_2$. *Angew. Chem., Int. Ed.* **2015**, *54*, 11016−11017.

(17) Solis-Ibarra, D.; Karunadasa, H. I. Reversible and Irreversible Chemisorption in Nonporous-Crystalline Hybrids. *Angew. Chem., Int. Ed.* **2014**, *53*, 1039−1042.

(18) Mitzi, D. B.; Medeiros, D. R.; Malenfant, P. R. L. Intercalated Organic-Inorganic Perovskites Stabilized by Fluoroaryl-Aryl Interactions. *Inorg. Chem.* **2002**, *41*, 2134−2145.

(19) Tieke, B. Chemical Reactions in Perovskite-Type Layer Structures. *Mol. Cryst. Liq. Cryst. (1969-1991)* **1983**, *93*, 119−145.

(20) Billing, D. G.; Lemmerer, A. Inorganic-Organic Hybrid Materials Incorporating Primary Cyclic Ammonium Cations: The Lead Bromide and Chloride Series. *CrystEngComm* **2009**, *11*, 1549−1562.

(21) Lemmerer, A.; Billing, D. G. Effect of Heteroatoms in the Inorganic-Organic Layered Perovskite-Type Hybrids $[(ZC_nH_{2n}NH_3)_2PbI_4]$, n = 2, 3, 4, 5, 6; Z = OH, Br and I; and $[(H_3NC_2H_4S_2C_2H_4NH_3)PbI_4]$. *CrystEngComm* **2010**, *12*, 1290−1301.

(22) Li, Y. Y.; Lin, C. K.; Zheng, G. L.; Cheng, Z. Y.; You, H.; Wang, W. D.; Lin, J. Novel <110>-Oriented Organic−Inorganic Perovskite Compound Stabilized by *N*-(3-aminopropyl)imidazole with Improved Optical Properties. *Chem. Mater.* **2006**, *18*, 3463−3469.

(23) Mercier, N.; Louvain, N.; Bi, W. Structural Diversity and Retro-Crystal Engineering Analysis of Iodometalate Hybrids. *CrystEngComm* **2009**, *11*, 720−734.

(24) Kataoka, S.; Banerjee, S.; Kawai, A.; Kamimura, Y.; Choi, J.-C.; Kodaira, T.; Sato, K.; Endo, A. Layered Hybrid Perovskites with Micropores Created by Alkylammonium Functional Silsesquioxane Interlayers. *J. Am. Chem. Soc.* **2015**, *137*, 4158−4163.

(25) Calabrese, J.; Jones, N. L.; Harlow, R. L.; Herron, N.; Thorn, D. L.; Wang, Y. Preparation and Characterization of Layered Lead Halide Compounds. *J. Am. Chem. Soc.* **1991**, *113*, 2328−2330.

(26) Mitzi, D. B. Templating and Structural Engineering in Organic-Inorganic Perovskites. *J. Chem. Soc., Dalton Trans.* **2001**, 1−12.

(27) Kojima, A.; Teshima, K.; Shirai, Y.; Miyasaka, T. Organometal Halide Perovskites as Visible-Light Sensitizers for Photovoltaic Cells. *J. Am. Chem. Soc.* **2009**, *131*, 6050−6051.

(28) Im, J.-H.; Lee, C.-R.; Lee, J.-W.; Park, S.-W.; Park, N.-G. 6.5% Efficient Perovskite Quantum-Dot-Sensitized Solar Cell. *Nanoscale* **2011**, *3*, 4088−4093.

(29) Etgar, L.; Gao, P.; Xue, Z.; Peng, Q.; Chandiran, A. K.; Liu, B.; Nazeeruddin, M. K.; Grätzel, M. Mesoscopic $CH_3NH_3PbI_3/TiO_2$ Heterojunction Solar Cells. *J. Am. Chem. Soc.* **2012**, *134*, 17396−17399.

(30) Lee, M. M.; Teuscher, J.; Miyasaka, T.; Murakami, T. N.; Snaith, H. J. Efficient Hybrid Solar Cells Based on Meso-Superstructured Organometal Halide Perovskites. *Science* **2012**, *338*, 643−647.

(31) Saliba, M.; Matsui, T.; Seo, J.-Y.; Domanski, K.; Correa-Baena, J.-P.; Nazeeruddin, M. K.; Zakeeruddin, S. M.; Tress, W.; Abate, A.; Hagfeldt, A.; Grätzel, M. Cesium-Containing Triple Cation Perovskite Solar Cells: Improved Stability, Reproducibility and High Efficiency. *Energy Environ. Sci.* **2016**, *9*, 1989−1997.

(32) Deschler, F.; Price, M.; Pathak, S.; Klintberg, L. E.; Jarausch, D.-D.; Higler, R.; Hüttner, S.; Leijtens, T.; Stranks, S. D.; Snaith, H. J.; Atatüre, M.; Phillips, R. T.; Friend, R. H. High Photoluminescence Efficiency and Optically Pumped Lasing in Solution-Processed Mixed Halide Perovskite Semiconductors. *J. Phys. Chem. Lett.* **2014**, *5*, 1421−1426.

(33) Xing, G.; Mathews, N.; Lim, S. S.; Yantara, N.; Liu, X.; Sabba, D.; Grätzel, M.; Mhaisalkar, S.; Sum, T. C. Low-Temperature Solution-Processed Wavelength-Tunable Perovskites for Lasing. *Nat. Mater.* **2014**, *13*, 476−480.

(34) Tan, Z.-K.; Moghaddam, R. S.; Lai, M. L.; Docampo, P.; Higler, R.; Deschler, F.; Price, M.; Sadhanala, A.; Pazos, L. M.; Credgington, D.; Hanusch, F.; Bein, T.; Snaith, H. J.; Friend, R. H. Bright Light-Emitting Diodes Based on Organometal Halide Perovskite. *Nat. Nanotechnol.* **2014**, *9*, 687−692.

DOI: 10.1021/acs.chemmater.6b05395
Chem. Mater. 2017, 29, 1868−1884

(35) Kim, Y.-H.; Cho, H.; Heo, J. H.; Kim, T.-S.; Myoung, N.; Lee, C.-L.; Im, S. H.; Lee, T.-W. Multicolored Organic/Inorganic Hybrid Perovskite Light-Emitting Diodes. *Adv. Mater.* **2015**, *27*, 1248−1254.
(36) Hong, X.; Ishihara, T.; Nurmikko, A. V. Dielectric Confinement Effect on Excitons in PbI_4-Based Layered Semiconductors. *Phys. Rev. B: Condens. Matter Mater. Phys.* **1992**, *45*, 6961−6964.
(37) Ishihara, T. Optical Properties of PbI-Based Perovskite Structures. *J. Lumin.* **1994**, *60*−*61*, 269−274.
(38) Mitzi, D. B.; Chondroudis, K.; Kagan, C. R. Organic-Inorganic Electronics. *IBM J. Res. Dev.* **2001**, *45*, 29−45.
(39) Stranks, S. D.; Eperon, G. E.; Grancini, G.; Menelaou, C.; Alcocer, M. J. P.; Leijtens, T.; Herz, L. M.; Petrozza, A.; Snaith, H. J. Electron-Hole Diffusion Lengths Exceeding 1 Micrometer in an Organometal Trihalide Perovskite Absorber. *Science* **2013**, *342*, 341−344.
(40) Muljarov, E. A.; Tikhodeev, S. G.; Gippius, N. A.; Ishihara, T. Excitons in Self-Organized Semiconductor/Insulator Superlattices: PbI-Based Perovskite Compounds. *Phys. Rev. B: Condens. Matter Mater. Phys.* **1995**, *51*, 14370−14378.
(41) Gauthron, K.; Lauret, J.-S.; Doyennette, L.; Lanty, G.; Al Choueiry, A.; Zhang, S. J.; Brehier, A.; Largeau, L.; Mauguin, O.; Bloch, J.; Deleporte, E. Optical Spectroscopy of Two-Dimensional Layered $(C_6H_5C_2H_4\text{-}NH_3)_2PbI_4$ Perovskite. *Opt. Express* **2010**, *18*, 5912−5919.
(42) Era, M.; Morimoto, S.; Tsutsui, T.; Saito, S. Organic-Inorganic Heterostructure Electroluminescent Device Using a Layered Perovskite Semiconductor $(C_6H_5C_2H_4NH_3)_2PbI_4$. *Appl. Phys. Lett.* **1994**, *65*, 676−678.
(43) Williams, R. T.; Song, K. S. The Self-Trapped Exciton. *J. Phys. Chem. Solids* **1990**, *51*, 679−716.
(44) Dohner, E. R.; Jaffe, A.; Bradshaw, L. R.; Karunadasa, H. I. Intrinsic White-Light Emission from Layered Hybrid Perovskites. *J. Am. Chem. Soc.* **2014**, *136*, 13154−13157.
(45) Hu, T.; Smith, M. D.; Dohner, E. R.; Sher, M.-J.; Wu, X.; Trinh, M. T.; Fisher, A.; Corbett, J.; Zhu, X.-Y.; Karunadasa, H. I.; Lindenberg, A. M. Mechanism for Broadband White-Light Emission from Two-Dimensional (110) Hybrid Perovskites. *J. Phys. Chem. Lett.* **2016**, *7*, 2258−2263.
(46) Moritomo, Y.; Tokura, Y. Pressure-Induced Disappearance of the In-Plane Lattice Distortion in Layered Cupric Chloride: $(C_2H_5NH_3)_2CuCl_4$. *J. Chem. Phys.* **1994**, *101*, 1763−1766.
(47) Jaffe, A.; Lin, Y.; Mao, W. L.; Karunadasa, H. I. Pressure-Induced Conductivity and Yellow-to-Black Piezochromism in a Layered Cu−Cl Hybrid Perovskite. *J. Am. Chem. Soc.* **2015**, *137*, 1673−1678.
(48) Gupta, S.; Pandey, T.; Singh, A. K. Suppression of Jahn−Teller Distortions and Origin of Piezochromism and Thermochromism in Cu−Cl Hybrid Perovskite. *Inorg. Chem.* **2016**, *55*, 6817−6824.
(49) Slavney, A. H.; Smaha, R. W.; Smith, I. C.; Jaffe, A.; Umeyama, D.; Karunadasa, H. I. Chemical Approaches to Addressing the Instability and Toxicity of Lead−Halide Perovskite Absorbers. *Inorg. Chem.* **2017**, *56*, 46−55.
(50) Needham, G. F.; Willett, R. D.; Franzen, H. F. Phase Transitions in Crystalline Models of Bilayers. 1. Differential Scanning Calorimetric and X-Ray Studies of $(C_{12}H_{25}NH_3)_2MCl_4$ and $(C_{14}H_{29}NH_3)_2MCl_4$ salts (M = Mn^{2+}, Cd^{2+}, Cu^{2+}). *J. Phys. Chem.* **1984**, *88*, 674−680.
(51) Dolzhenko, Y. I.; Inabe, T.; Maruyama, Y. In Situ X-Ray Observation on the Intercalation of Weak Interaction Molecules into Perovskite-Type Layered Crystals $(C_9H_{19}NH_3)_2PbI_4$ and $(C_{10}H_{21}NH_3)_2CdCl_4$. *Bull. Chem. Soc. Jpn.* **1986**, *59*, 563−567.
(52) Smith, M. D.; Pedesseau, L.; Kepenekian, M.; Smith, I. C.; Katan, C.; Even, J.; Karunadasa, H. I. Decreasing the Electronic Confinement in Layered Perovskites Through Intercalation. *Chem. Sci.* **2017**, DOI: 10.1039/C6SC02848A.
(53) Papavassiliou, G. C.; Koutselas, I. B.; Terzis, A.; Whangbo, M.-H. Structural and Electronic Properties of the Natural Quantum-Well System $(C_6H_5CH_2CH_2NH_3)_2SnI_4$. *Solid State Commun.* **1994**, *91*, 695−698.
(54) Billing, D. G.; Lemmerer, A. Synthesis, Characterization and Phase Transitions in the Inorganic-Organic Layered Perovskite-Type Hybrids $[(C_nH_{2n+1}NH_3)_2PbI_4]$, *n* = 4, 5 and 6. *Acta Crystallogr., Sect. B: Struct. Sci.* **2007**, *63*, 735−747.
(55) Castro-Castro, L. M.; Guloy, A. M. Organic-Based Layered Perovskites of Mixed-Valent Gold(I)/Gold(III) Iodides. *Angew. Chem., Int. Ed.* **2003**, *42*, 2771−2774.
(56) Mitzi, D. B.; Dimitrakopoulos, C. D.; Kosbar, L. L. Structurally Tailored Organic-Inorganic Perovskites: Optical Properties and Solution-Processed Channel Materials for Thin-Film Transistors. *Chem. Mater.* **2001**, *13*, 3728−3740.
(57) Even, J.; Pedesseau, L.; Katan, C. Understanding Quantum Confinement of Charge Carriers in Layered 2D Hybrid Perovskites. *ChemPhysChem* **2014**, *15*, 3733−3741.
(58) Takagi, H.; Kunugita, H.; Ema, K. Influence of the Image Charge Effect on Excitonic Energy Structure in Organic−Inorganic Multiple Quantum Well Crystals. *Phys. Rev. B: Condens. Matter Mater. Phys.* **2013**, *87*, 125421.
(59) Hong, X.; Ishihara, T.; Nurmikko, A. V. Photoconductivity and Electroluminescence in Lead Iodide Based Natural Quantum-Well Structures. *Solid State Commun.* **1992**, *84*, 657−661.
(60) Shinada, M.; Sugano, S. Interband Optical Transitions in Extremely Anisotropic Semiconductors. I. Bound and Unbound Exciton Absorption. *J. Phys. Soc. Jpn.* **1966**, *21*, 1936−1946.
(61) Keldysh, L. V. Coulomb Interaction in Thin Films of Semiconductors and Semimetals. *Pis'ma Zh. Eksp. Teor. Fiz.* **1979**, *29*, 716−719.
(62) Hanamura, E.; Nagaosa, N.; Kumagai, M.; Takagahara, T. Quantum Wells with Enhanced Exciton Effects and Optical Non-Linearity. *Mater. Sci. Eng., B* **1988**, *1*, 255−258.
(63) Hong, X.; Ishihara, T.; Nurmikko, A. V. Dielectric Confinement Effect on Excitons in PbI_4-Based Layered Semiconductors. *Phys. Rev. B: Condens. Matter Mater. Phys.* **1992**, *45*, 6961−6964.
(64) Sourisseau, S.; Louvain, N.; Bi, W.; Mercier, N.; Rondeau, D.; Boucher, F.; Buzaré, J.-Y.; Legein, C. Reduced Band Gap Hybrid Perovskites Resulting from Combined Hydrogen and Halogen Bonding at the Organic-Inorganic Interface. *Chem. Mater.* **2007**, *19*, 600−607.
(65) Katan, C.; Pedesseau, L.; Kepenekian, M.; Rolland, A.; Even, J. Interplay of Spin-Orbit Coupling and Lattice Distortion in Metal Substituted 3D Tri-Chloride Hybrid Perovskites. *J. Mater. Chem. A* **2015**, *3*, 9232−9240.
(66) Winter, M.; Besenhard, J. O.; Spahr, M. E.; Novák, P. Insertion Electrode Materials for Rechargeable Lithium Batteries. *Adv. Mater.* **1998**, *10*, 725−763.
(67) Jaffe, A.; Karunadasa, H. I. Lithium Cycling in a Self-Assembled Copper Chloride−Polyether Hybrid Electrode. *Inorg. Chem.* **2014**, *53*, 6494−6496.
(68) Xia, H.-R.; Sun, W.-T.; Peng, L.-M. Hydrothermal Synthesis of Organometal Halide Perovskites for Li-Ion Batteries. *Chem. Commun.* **2015**, *51*, 13787−13790.
(69) Yang, T.-Y.; Gregori, G.; Pellet, N.; Grätzel, M.; Maier, J. The Significance of Ion Conduction in a Hybrid Organic−Inorganic Lead-Iodide-Based Perovskite Photosensitizer. *Angew. Chem., Int. Ed.* **2015**, *54*, 7905−7910.
(70) Tieke, B.; Chapuis, G. Solid-State Polymerization of Butadienes. Crystal Structure and Solution Properties of a Stereoregular Amphoteric 1,4-*Trans*-Polybutadiene. *J. Polym. Sci., Polym. Chem. Ed.* **1984**, *22*, 2895−2921.
(71) Tieke, B.; Chapuis, G. Solid State Polymerization of Butadienes in Layer Structures. *Mol. Cryst. Liq. Cryst. (1969-1991)* **1986**, *137*, 101−116.
(72) Green, B. S.; Lahav, M.; Schmidt, G. M. J. Topochemistry. Part XXXI. Formation of Cyclo-octa-1,5-*cis*,*cis*-dienes from 1,4-disubstituted s-*trans*-Butadienes in the Solid State. A Contribution to the Problem of C4- *versus* C8-Cyclodimerisation. *J. Chem. Soc. B* **1971**, 1552−1564.

DOI: 10.1021/acs.chemmater.6b05395
Chem. Mater. 2017, 29, 1868−1884

(73) Lahav, M.; Schmidt, G. M. J. Topochemistry. Part XXIII. The Solid-State Photochemistry at 25° of Some Muconic Acid Derivatives. *J. Chem. Soc. B* **1967**, *0*, 312−317.
(74) Yao, K.; Wang, X.; Xu, Y.-x.; Li, F.; Zhou, L. Multilayered Perovskite Materials Based on Polymeric-Ammonium Cations for Stable Large-Area Solar Cell. *Chem. Mater.* **2016**, *28*, 3131−3138.
(75) Dincă, M.; Long, J. R. Hydrogen Storage in Microporous Metal−Organic Frameworks with Exposed Metal Sites. *Angew. Chem., Int. Ed.* **2008**, *47*, 6766−6779.
(76) Demessence, A.; D'Alessandro, D. M.; Foo, M. L.; Long, J. R. Strong CO_2 Binding in a Water-Stable, Triazolate-Bridged Metal−Organic Framework Functionalized with Ethylenediamine. *J. Am. Chem. Soc.* **2009**, *131*, 8784−8786.
(77) Carey, F. A.; Sundberg, R. J. *Advanced Organic Chemistry, Part B: Reactions and Synthesis*, Fourth ed.; Springer: New York, 2001; pp 200−206.
(78) Strominger, D.; Hollander, J. M.; Seaborg, G. T. Table of Isotopes. *Rev. Mod. Phys.* **1958**, *30*, 585−904.
(79) Haefner, D. R.; Tranter, T. J. *Methods of Gas Phase Capture of Iodine from Fuel Reprocessing Off-Gas: a Literature Survey*; Idaho National Laboratory: Idaho Falls, ID, 2007.
(80) Chapman, K. W.; Chupas, P. J.; Nenoff, T. M. Radioactive Iodine Capture in Silver-Containing Mordenites through Nanoscale Silver Iodide Formation. *J. Am. Chem. Soc.* **2010**, *132*, 8897−8899.
(81) Westphal, B.; Cummings, D. G.; Giglio, J. J.; Wahlquist, D. L.; Bateman, K. J.; McCartin, W. M.; Park, J. J.; Shin, J. M.; Begg, B. D. Capture and Sequestration of Radioactive Iodine. *MRS Online Proc. Libr.* **2010**, *1265*, 1265−AA02−04.
(82) Sava, D. F.; Chapman, K. W.; Rodriguez, M. A.; Greathouse, J. A.; Crozier, P. S.; Zhao, H.; Chupas, P. J.; Nenoff, T. M. Competitive I_2 Sorption by Cu-BTC from Humid Gas Streams. *Chem. Mater.* **2013**, *25*, 2591−2596.
(83) Field, K. W.; Wilder, D.; Utz, A.; Kolb, K. E. Addition of Iodine to Alkenes: A Pseudo-First-, Second-, or Third-Order Kinetics Experiment. *J. Chem. Educ.* **1987**, *64*, 269−271.
(84) Solis-Ibarra, D.; Smith, I. C.; Karunadasa, H. I. Post-Synthetic Halide Conversion and Selective Halogen Capture in Hybrid Perovskites. *Chem. Sci.* **2015**, *6*, 4054−4059.
(85) Downs, A. J.; Adams, C. J. *The Chemistry of Chlorine, Bromine, Iodine, and Astatine*; Elsevier Ltd: Amsterdam, 1973; pp 1107−1594.
(86) Pavelka, S. Metabolism of Bromide and its Interference with the Metabolism of Iodine. *Physiol. Res.* **2004**, *53* (Suppl 1), S81−S90.
(87) Vanýsek, P. *CRC Handbook of Chemistry and Physics*, 95th ed.; Haynes, W. M., Ed.; Taylor & Francis Group: Boca Raton, FL, 2014; pp 5-80−5-89.
(88) Poutsma, M. L. Chlorination Studies of Unsaturated Materials in Nonpolar Media. IV. The Ionic Pathway for Alkylated Ethylenes. Products and Relative Reactivities. *J. Am. Chem. Soc.* **1965**, *87*, 4285−4293.
(89) Ruasse, M. F.; Zhang, B. L. The Nucleophilic Contribution of the Solvent in Olefin Bromination. I. Steric Inhibition to Nucleophilic Solvation in Alkene Bromination via Brominium Ions. *J. Org. Chem.* **1984**, *49*, 3207−3210.
(90) Ruasse, M. F.; Lefebvre, E. The Nucleophilic Contribution of the Solvent in Olefin Bromination. II. Reactivity Dependence of the Nucleophilic Solvation in Bromination via β-Bromo Carbocations. *J. Org. Chem.* **1984**, *49*, 3210−3212.
(91) Teberekidis, V. I.; Sigalas, M. P. Density Functional Study of Potential Energy Surfaces and Relative Stabilities of Halonium Cations of Ethylene and Cyclopentenes. *Tetrahedron* **2002**, *58*, 6171−6178.
(92) Teberekidis, V. I.; Sigalas, M. P. Structure and Stability of Halonium Cations of Cycloalkenes. A Theoretical Study. *Tetrahedron* **2003**, *59*, 4749−4756.
(93) Teberekidis, V. I.; Sigalas, M. P. Ab initio and Density Functional Study of Substituent Effects in Halogenated Cations of Alkenes. *Tetrahedron* **2005**, *61*, 3967−3976.
(94) Friedel, C. Ueber die Einwirkung des Broms auf den Isopropylalkohol und auf das Isopropyljodür. *Ann. Chem. Pharm.* **1865**, *135*, 203−207.
(95) Corey, E. J.; Wechter, W. J. The Stereochemistry of the Non-Radical Halogen Exchange between Active Sec-Octyl Iodide and Chlorine. *J. Am. Chem. Soc.* **1954**, *76*, 6040−6042.
(96) Manser, J. S.; Christians, J. A.; Kamat, P. V. Intriguing Optoelectronic Properties of Metal Halide Perovskites. *Chem. Rev.* **2016**, *116*, 12956−13008.
(97) Shockley, W.; Queisser, H. J. Detailed Balance Limit of Efficiency of *p-n* Junction Solar Cells. *J. Appl. Phys.* **1961**, *32*, 510−519.
(98) Edri, E.; Kirmayer, S.; Cahen, D.; Hodes, G. High Open-Circuit Voltage Solar Cells Based on Organic−Inorganic Lead Bromide Perovskite. *J. Phys. Chem. Lett.* **2013**, *4*, 897−902.
(99) Cho, H.; Jeong, S.-H.; Park, M.-H.; Kim, Y.-H.; Wolf, C.; Lee, C.-L.; Heo, J. H.; Sadhanala, A.; Myoung, N.; Yoo, S.; Im, S. H.; Friend, R. H.; Lee, T.-W. Overcoming the Electroluminescence Efficiency Limitations of Perovskite Light-Emitting Diodes. *Science* **2015**, *350*, 1222−1225.
(100) Edri, E.; Kirmayer, S.; Kulbak, M.; Hodes, G.; Cahen, D. Chloride Inclusion and Hole Transport Material Doping to Improve Methyl Ammonium Lead Bromide Perovskite-Based High Open-Circuit Voltage Solar Cells. *J. Phys. Chem. Lett.* **2014**, *5*, 429−433.
(101) Heo, J. H.; Song, D. H.; Im, S. H. Planar $CH_3NH_3PbBr_3$ Hybrid Solar Cells with 10.4% Power Conversion Efficiency, Fabricated by Controlled Crystallization in the Spin-Coating Process. *Adv. Mater.* **2014**, *26*, 8179−8183.
(102) Kim, M.-c.; Kim, B. J.; Son, D.-Y.; Park, N.-G.; Jung, H. S.; Choi, M. Observation of Enhanced Hole Extraction in Br Concentration Gradient Perovskite Materials. *Nano Lett.* **2016**, *16*, 5756−5763.
(103) Hoke, E. T.; Slotcavage, D. J.; Dohner, E. R.; Bowring, A. R.; Karunadasa, H. I.; McGehee, M. D. Reversible Photo-Induced Trap Formation in Mixed-Halide Hybrid Perovskites for Photovoltaics. *Chem. Sci.* **2015**, *6*, 613−617.
(104) Li, G.; Ho, J. Y.-L.; Wong, M.; Kwok, H. S. Reversible Anion Exchange Reaction in Solid Halide Perovskites and Its Implication in Photovoltaics. *J. Phys. Chem. C* **2015**, *119*, 26883−26888.
(105) Pellet, N.; Teuscher, J.; Maier, J.; Grätzel, M. Transforming Hybrid Organic Inorganic Perovskites by Rapid Halide Exchange. *Chem. Mater.* **2015**, *27*, 2181−2188.
(106) Chen, K.; Deng, X.; Goddard, R.; Tüysüz, H. Pseudomorphic Transformation of Organometal Halide Perovskite Using the Gaseous Hydrogen Halide Reaction. *Chem. Mater.* **2016**, *28*, 5530−5537.
(107) Zhao, Y.; Zhu, K. Optical Bleaching of Perovskite (CH_3NH_3)-PbI_3 Through Room-Temperature Phase Transformation Induced by Ammonia. *Chem. Commun.* **2014**, *50*, 1605−1607.
(108) Zhou, Z.; Wang, Z.; Zhou, Y.; Pang, S.; Wang, D.; Xu, H.; Liu, Z.; Padture, N. P.; Cui, G. Methylamine-Gas-Induced Defect-Healing Behavior of $CH_3NH_3PbI_3$ Thin Films for Perovskite Solar Cells. *Angew. Chem., Int. Ed.* **2015**, *54*, 9705−9709.
(109) Raga, S. R.; Ono, L. K.; Qi, Y. Rapid Perovskite Formation by CH_3NH_2 Gas-Induced Intercalation and Reaction of PbI_2. *J. Mater. Chem. A* **2016**, *4*, 2494−2500.
(110) Grochala, W.; Hoffmann, R.; Feng, J.; Ashcroft, N. W. The Chemical Imagination at Work in *Very* Tight Places. *Angew. Chem., Int. Ed.* **2007**, *46*, 3620−3642.
(111) Hemley, R. J.; Percy, W. Bridgman's Second Century. *High Pressure Res.* **2010**, *30*, 581−619.
(112) Luty, T.; Eckhardt, C. J. General Theoretical Concepts for Solid State Reactions: Quantitative Formulation of the Reaction Cavity, Steric Compression, and Reaction-Induced Stress Using an Elastic Multipole Representation of Chemical Pressure. *J. Am. Chem. Soc.* **1995**, *117*, 2441−2452.
(113) Onoda-Yamamuro, N.; Yamamuro, O.; Matsuo, T.; Suga, H. *p-T* Phase Relations of $CH_3NH_3PbX_3$ (X = Cl, Br, I) Crystals. *J. Phys. Chem. Solids* **1992**, *53*, 277−281.
(114) Gesi, K. Effect of Hydrostatic Pressure on the Structural Phase Transitions in $CH_3NH_3PbX_3$ (X = Cl, Br, I). *Ferroelectrics* **1997**, *203*, 249−268.

DOI: 10.1021/acs.chemmater.6b05395
Chem. Mater. 2017, 29, 1868−1884

(115) Swainson, I. P.; Tucker, M. G.; Wilson, D. J.; Winkler, B.; Milman, V. Pressure Response of an Organic-Inorganic Perovskite: Methylammonium Lead Bromide. *Chem. Mater.* **2007**, *19*, 2401−2405.
(116) Matsuishi, K.; Ishihara, T.; Onari, S.; Chang, Y. H.; Park, C. H. Optical Properties and Structural Phase Transitions of Lead-Halide Based Inorganic−Organic 3D and 2D Perovskite Semiconductors Under High Pressure. *Phys. Status Solidi B* **2004**, *241*, 3328−3333.
(117) Lee, Y.; Mitzi, D. B.; Barnes, P. W.; Vogt, T. Pressure-Induced Phase Transitions and Templating Effect in Three-Dimensional Organic-Inorganic Hybrid Perovskites. *Phys. Rev. B: Condens. Matter Mater. Phys.* **2003**, *68*, No. 020103(R).
(118) Wang, Y.; Lü, X.; Yang, W.; Wen, T.; Yang, L.; Ren, X.; Wang, L.; Lin, Z.; Zhao, Y. Pressure-Induced Phase Transformation, Reversible Amorphization, and Anomalous Visible Light Response in Organolead Bromide Perovskite. *J. Am. Chem. Soc.* **2015**, *137*, 11144−11149.
(119) Ou, T.; Yan, J.; Xiao, C.; Shen, W.; Liu, C.; Liu, X.; Han, Y.; Ma, Y.; Gao, C. Visible Light Response, Electrical Transport, and Amorphization in Compressed Organolead Iodine Perovskites. *Nanoscale* **2016**, *8*, 11426−11431.
(120) Jaffe, A.; Lin, Y.; Beavers, C. M.; Voss, J.; Mao, W. L.; Karunadasa, H. I. High-Pressure Single-Crystal Structures of 3D Lead-Halide Hybrid Perovskites and Pressure Effects on their Electronic and Optical Properties. *ACS Cent. Sci.* **2016**, *2*, 201−209.
(121) Jiang, S.; Fang, Y.; Li, R.; Xiao, H.; Crowley, J.; Wang, C.; White, T. J.; Goddard, W. A.; Wang, Z.; Baikie, T.; Fang, J. Pressure-Dependent Polymorphism and Band-Gap Tuning of Methylammonium Lead Iodide Perovskite. *Angew. Chem., Int. Ed.* **2016**, *55*, 6540−6544.
(122) Capitani, F.; Marini, C.; Caramazza, S.; Postorino, P.; Garbarino, G.; Hanfland, M.; Pisanu, A.; Quadrelli, P.; Malavasi, L. High-Pressure Behavior of Methylammonium Lead Iodide ($MAPbI_3$) Hybrid Perovskite. *J. Appl. Phys.* **2016**, *119*, 185901.
(123) Wang, L.; Wang, K.; Zou, B. Pressure-Induced Structural and Optical Properties of Organometal Halide Perovskite-Based Formamidinium Lead Bromide. *J. Phys. Chem. Lett.* **2016**, *7*, 2556−2562.
(124) Kong, L.; Liu, G.; Gong, J.; Hu, Q.; Schaller, R. D.; Dera, P.; Zhang, D.; Liu, Z.; Yang, W.; Zhu, K.; Tang, Y.; Wang, C.; Wei, S.-H.; Xu, T.; Mao, H.-k. Simultaneous Band-Gap Narrowing and Carrier-Lifetime Prolongation of Organic−Inorganic Trihalide Perovskites. *Proc. Natl. Acad. Sci. U. S. A.* **2016**, *113*, 8910−8915.
(125) Szafrański, M.; Katrusiak, A. Mechanism of Pressure-Induced Phase Transitions, Amorphization, and Absorption-Edge Shift in Photovoltaic Methylammonium Lead Iodide. *J. Phys. Chem. Lett.* **2016**, *7*, 3458−3466.
(126) Lü, X.; Wang, Y.; Stoumpos, C. C.; Hu, Q.; Guo, X.; Chen, H.; Yang, L.; Smith, J. S.; Yang, W.; Zhao, Y.; Xu, H.; Kanatzidis, M. G.; Jia, Q. Enhanced Structural Stability and Photo Responsiveness of $CH_3NH_3SnI_3$ Perovskite via Pressure-Induced Amorphization and Recrystallization. *Adv. Mater.* **2016**, *28*, 8663−8668.
(127) Noh, J. H.; Im, S. H.; Heo, J. H.; Mandal, T. N.; Seok, S. I. Chemical Management for Colorful, Efficient, and Stable Inorganic−Organic Hybrid Nanostructured Solar Cells. *Nano Lett.* **2013**, *13*, 1764−1769.
(128) Stoumpos, C. C.; Malliakas, C. D.; Kanatzidis, M. G. Semiconducting Tin and Lead Iodide Perovskites with Organic Cations: Phase Transitions, High Mobilities, and Near-Infrared Photoluminescent Properties. *Inorg. Chem.* **2013**, *52*, 9019−9038.
(129) Saidaminov, M. I.; Abdelhady, A. L.; Murali, B.; Alarousu, E.; Burlakov, V. M.; Peng, W.; Dursun, I.; Wang, L.; He, Y.; Maculan, G.; Goriely, A.; Wu, T.; Mohammed, O. F.; Bakr, O. M. High-Quality Bulk Hybrid Perovskite Single Crystals Within Minutes by Inverse Temperature Crystallization. *Nat. Commun.* **2015**, *6*, 7586.
(130) Kuku, T. A.; Salau, A. M. Electrical Conductivity of $CuSnI_3$, $CuPbI_3$ and $KPbI_3$. *Solid State Ionics* **1987**, *25*, 1−7.
(131) Yang, T.-Y.; Gregori, G.; Pellet, N.; Grätzel, M.; Maier, J. The Significance of Ion Conduction in a Hybrid Organic−Inorganic Lead-Iodide-Based Perovskite Photosensitizer. *Angew. Chem., Int. Ed.* **2015**, *54*, 7905−7910.
(132) Eames, C.; Frost, J. M.; Barnes, P. R. F.; O'Regan, B. C.; Walsh, A.; Islam, M. S. Ionic Transport in Hybrid Lead Iodide Perovskite Solar Cells. *Nat. Commun.* **2015**, *6*, 7497.
(133) Murayama, C.; Iye, Y.; Enomoto, T.; Môri, N.; Yamada, Y.; Matsumoto, T.; Kubo, Y.; Shimakawa, Y.; Manako, T. Correlation Between the Pressure-Induced Changes in the Hall Coefficient and T_c in Superconducting Cuprates. *Phys. C* **1991**, *183*, 277−285.
(134) Schilling, J. S. In *Frontiers of High Pressure Research II: Application of High Pressure to Low-Dimensional Novel Electronic Materials*; Hochheimer, H. D., Kuchta, B., Dorhout, P. K., Yarger, J. L., Eds.; Springer: New York, 2001; Vol. *48*, pp 345−360.
(135) Valiente, R.; Rodríguez, F. Electron-Phonon Coupling in Charge-Transfer and Crystal-Field States of Jahn−Teller $CuCl_6^{4-}$ Systems. *Phys. Rev. B: Condens. Matter Mater. Phys.* **1999**, *60*, 9423−9429.
(136) Ohwada, K.; Ishii, K.; Inami, T.; Murakami, Y.; Shobu, T.; Ohsumi, H.; Ikeda, N.; Ohishi, Y. Structural Properties and Phase Transition of Hole-Orbital-Ordered $(C_2H_5NH_3)_2CuCl_4$ Studied by Resonant and Non-Resonant X-Ray Scatterings Under High Pressure. *Phys. Rev. B: Condens. Matter Mater. Phys.* **2005**, *72*, 014123.
(137) Rodríguez, F.; Aguado, F.; Valiente, R.; Hanfland, M.; Itiè, J. P. Variation of the Jahn−Teller Distortion with Pressure in Perovskite Layers A_2CuCl_4. Influence on the Charge-Transfer Band. *Phys. Status Solidi B* **2007**, *244*, 156−161.
(138) Aguado, F.; Rodríguez, F.; Valiente, R.; Itiè, J.-P.; Hanfland, M. Pressure Effects on Jahn−Teller Distortion in Perovskites: The Roles of Local and Bulk Compressibilities. *Phys. Rev. B: Condens. Matter Mater. Phys.* **2012**, *85*, 100101.
(139) Desjardins, S. R.; Wilcox, D. E.; Musselman, R. L.; Solomon, E. I. Polarized, Single-Crystal, Electronic Spectral Studies of $Cu_2Cl_6^{2-}$: Excited-State Effects of the Binuclear Interaction. *Inorg. Chem.* **1987**, *26*, 288−300.
(140) Matsuishi, K.; Suzuki, T.; Onari, S.; Gregoryanz, E.; Hemley, R. J.; Mao, H. K. Excitonic States of Alkylammonium Lead-Iodide Layered Perovskite Semiconductors Under Hydrostatic Pressure to 25 GPa. *Phys. Status Solidi B* **2001**, *223*, 177−182.
(141) Xiao, Z.; Meng, W.; Saparov, B.; Duan, H.-S.; Wang, C.; Feng, C.; Liao, W.; Ke, W.; Zhao, D.; Wang, J.; Mitzi, D. B.; Yan, Y. Photovoltaic Properties of Two-Dimensional $(CH_3NH_3)_2Pb(SCN)_2I_2$ Perovskite: A Combined Experimental and Density Functional Theory Study. *J. Phys. Chem. Lett.* **2016**, *7*, 1213−1218.
(142) Umeyama, D.; Lin, Y.; Karunadasa, H. I. Red-to-Black Piezochromism in a Compressible Pb−I−SCN Layered Perovskite. *Chem. Mater.* **2016**, *28*, 3241−3244.
(143) McMeekin, D. P.; Sadoughi, G.; Rehman, W.; Eperon, G. E.; Saliba, M.; Hörantner, M. T.; Haghighirad, A.; Sakai, N.; Korte, L.; Rech, B.; Johnston, M. B.; Herz, L. M.; Snaith, H. J. A Mixed-Cation Lead Mixed-Halide Perovskite Absorber for Tandem Solar Cells. *Science* **2016**, *351*, 151−155.
(144) Slotcavage, D. J.; Karunadasa, H. I.; McGehee, M. D. Light-Induced Phase Segregation in Halide-Perovskite Absorbers. *ACS Energy Lett.* **2016**, *1*, 1199−1205.
(145) Bellitto, C.; Day, P. Magnetic Susceptibility and Optical Spectra of the Organic-Intercalated Two-Dimensional Ferromagnets Bis(monomethylammonium)- and Bis(monoethylammonium) Tetrachlorochromate(II). *J. Chem. Soc., Dalton Trans.* **1978**, 1207−1212.
(146) Watanabe, N.; Kojima, N.; Ban, T.; Tsujikawa, I. Optical Absorption Spectra in the Quasi-Two-Dimensional Antiferromagnets $(NH_3(CH_2)_nNH_3)MnCl_4$ (n = 2, 3, 4, 5): I. Experimental. *J. Phys. C: Solid State Phys.* **1988**, *21*, 4795−4808.

DOI: 10.1021/acs.chemmater.6b05395
Chem. Mater. 2017, 29, 1868−1884